RESEARCH ARTICLE

Molecular and functional analysis of calcium binding by a cancer-linked calreticulin mutant

Ishmael Nii Ayibontey Tagoe[1,2], Amanpreet Kaur[1], Osbourne Quaye[2], Emmanuel Ayitey Tagoe[3], Nicole M Koropatkin[1], Leslie S Satin[4], Malini Raghavan[1]*

[1]Department of Microbiology and Immunology, University of Michigan Medical School, Ann Arbor, United States; [2]West African Centre for Cell Biology of Infectious Pathogens, Departments of Biochemistry, Cell and Molecular Biology, University of Ghana, Accra, Ghana; [3]Medical Laboratory Sciences, University of Ghana, Accra, Ghana; [4]Department of Pharmacology, University of Michigan Medical School, Ann Arbor, United States

eLife Assessment

This work makes an **important** contribution to understanding the role of calreticulin and the Del52 variant in calcium homeostasis in cells based on **convincing** evidence. There was some question as to whether the work in vitro fully recapitulated the physiological setting in which the Del52 variant has been reported to have defects in calcium homeostasis. Nonetheless, the studies are well performed using appropriate methods to address these questions and make a significant contribution to the understanding of calreticulin, and the Del52 variant, function in health and disease.

***For correspondence:** malinir@umich.edu

Competing interest: The authors declare that no competing interests exist.

Funding: See page 20

Preprint posted
05 November 2025
Sent for Review
05 November 2025
Reviewed preprint v1
22 January 2026
Reviewed preprint v2
22 September 2026
Version of Record
29 October 2026

Reviewing Editor: Michael L Dustin, University of Oxford, United Kingdom

© Copyright Tagoe *et al.* This article is distributed under the terms of the Creative Commons Attribution License, which permits unrestricted use and redistribution provided that the original author and source are credited.

Abstract Calreticulin (CRT) is an endoplasmic reticulum (ER) chaperone with low-affinity calcium-binding sites in its C-terminal domain. This region is altered by somatic mutations in the CRT gene (*CALR*), which drive a subset of myeloproliferative neoplasms (MPNs). Perturbations in ER calcium storage and signaling are reported for the MPN type I mutant, CRT_{Del52}, and are linked to disease pathogenesis. Using recombinant CRT proteins, we found similar low-affinity calcium-binding characteristics for wild-type CRT and CRT_{Del52}, as determined by isothermal titration calorimetry (ITC). Residues 340–349, conserved in both wild-type CRT and CRT_{Del52}, contribute to binding. Furthermore, ER and cytosolic calcium levels, and store-operated calcium entry (SOCE), were comparable in CRT knockout (CRT-KO) cells reconstituted with wild-type CRT or CRT_{Del52}. Notably, the CRT-KO induces expression of multiple ER proteins known to contain low-affinity calcium-binding sites or regulate ER calcium levels. Overall, these findings indicate that CRT_{Del52} retains at least some low-affinity calcium-binding capacity and that CRT deficiency induces compensatory cellular changes that maintain ER calcium homeostasis.

Introduction

Calreticulin (CRT) is an endoplasmic reticulum (ER) luminal protein that plays key roles in the assembly and folding of N-linked glycoproteins. CRT has a single high-affinity calcium-binding site within a globular domain and a highly acidic C-terminal domain that contains multiple low-affinity calcium-binding sites (***Baksh and Michalak, 1991***; ***Wijeyesakere et al., 2011***). As an ER chaperone, CRT is thought to play a critical role in maintaining cellular calcium homeostasis (***Venkatesan et al., 2021b***; ***Michalak, 2024***). The ER has a relatively high free calcium concentration of 0.5–1 μM through the presence

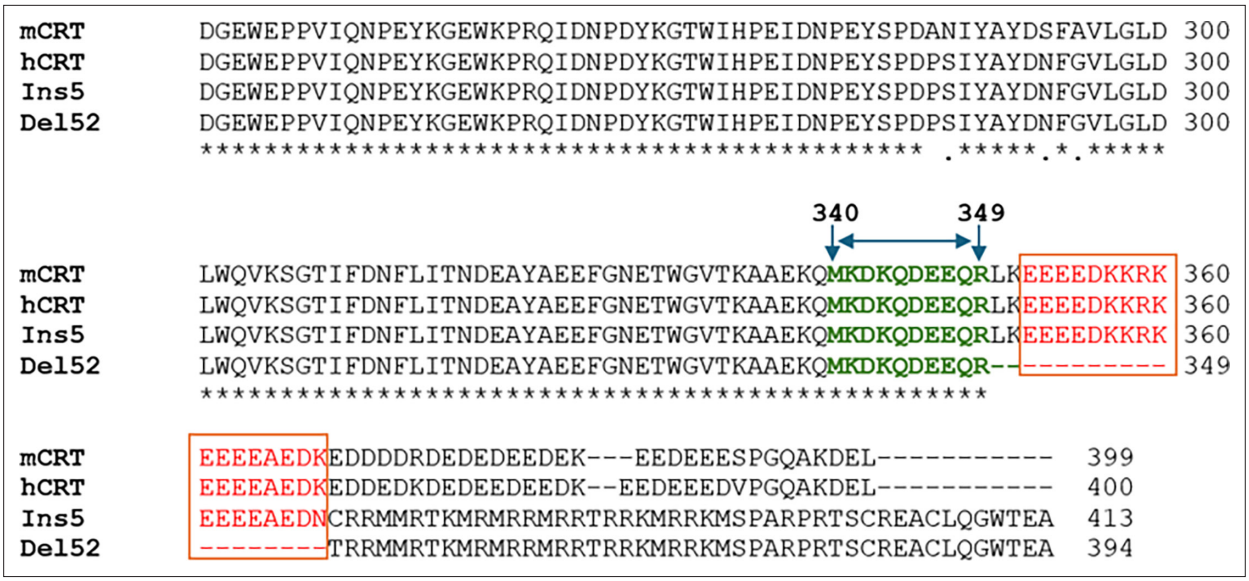


Figure 1. Sequence alignments of the C-terminal residues of murine and human calreticulin (mCRT and hCRT), and the myeloproliferative neoplasm (MPN)-linked CRT mutants Ins5 and Del52. Multiple sequence alignment using Clustal Omega was employed to compare C-domain sequences of mature mCRT, hCRT, Del52, and Ins5 proteins. Acidic residues (340–349) previously implicated in low-affinity calcium binding by mCRT that are shared between wild-type and both CRT_{Del52} and CRT_{Ins5} are highlighted in green. Additional acidic residues shared just between wild-type CRT and CRT_{Ins5} are shown in red. There are additional acidic residues unique to wild-type CRT. Mature protein numbering is used for the CRT sequences.

of various low-affinity calcium-binding proteins that buffer calcium, whereas cytosolic calcium levels are maintained within a narrow range of around 100 nM (***Michalak, 2024***). The maintenance of calcium homeostasis within cellular compartments is essential for cell function and survival (***Bagur and Hajnóczky, 2017***). Early studies have shown that the C-domain of CRT contributes to ER calcium storage, although free ER luminal concentrations are unchanged (***Nakamura et al., 2001***).

Somatic mutations of exon 9 of the *CALR* gene, including a 52-base pair deletion (Del52; type I mutation) and a 5-base pair insertion (Ins5; type II mutation), are driver mutations in some myeloproliferative neoplasms (MPNs), specifically in essential thrombocythemia and primary and secondary myelofibrosis (***Klampfl et al., 2013***; ***Nangalia et al., 2013***). The MPN mutations change the CRT C-domain residues from being predominantly acidic to a high prevalence of basic amino acids and result in a loss of the ER-retention KDEL sequence (***Klampfl et al., 2013***; ***Nangalia et al., 2013***; ***Figure 1***). Although all MPN CRT mutants change the sequence and charge of the C-domain, a greater number of acidic residues are retained in MPN type II mutant (CRT_{Ins5}), compared to the type I mutant (CRT_{Del52}) (***Figure 1***). The loss of more acidic residues from the C-terminal domain of CRT_{Del52} has been reported to impair its calcium binding and reduce ER calcium levels (***Ibarra et al., 2022***). Store-operated calcium entry (SOCE) is a physiological process that allows for the entry of extracellular calcium and ER calcium restoration following ER calcium depletion (***Putney, 2011***; ***Zhang et al., 2020***). Altered calcium release from the ER and SOCE was reported for MPN type I but not type II mutants in cultured megakaryocytes from MPN patients (***Pietra et al., 2016***). In another study, spontaneous calcium spikes and increased SOCE activation were observed in cultured megakaryocytes from MPN type I and type II patients when compared to healthy donors (***Di Buduo et al., 2020***).

Although global calcium-binding defects were predicted or qualitatively measured for CRT_{Del52} (***Shivarov et al., 2014***; ***Ibarra et al., 2022***), and altered cellular calcium signaling is also reported (***Pietra et al., 2016***; ***Di Buduo et al., 2020***), it remains unclear whether MPN-linked CRT_{Del52} has any low-affinity calcium-binding capacity, given that a few conserved acidic residues are retained in its C-domain (***Figure 1***). In fact, our previous studies showed that a truncated version of murine wild-type CRT (mCRT) containing the non-mutated part of CRT_{Del52} and two additional C-terminal residues ($mCRT_{1–351}$) showed similar low-affinity calcium-binding characteristics as the wild-type mCRT (***Wijeyesakere et al., 2011***). On the other hand, further truncation of mCRT ($mCRT_{1–339}$) was needed to disrupt calcium binding (***Wijeyesakere et al., 2011***; ***Wijeyesakere et al., 2016***). The goal of the current study was to quantitatively measure low-affinity calcium binding by CRT_{Del52} compared with wild-type human

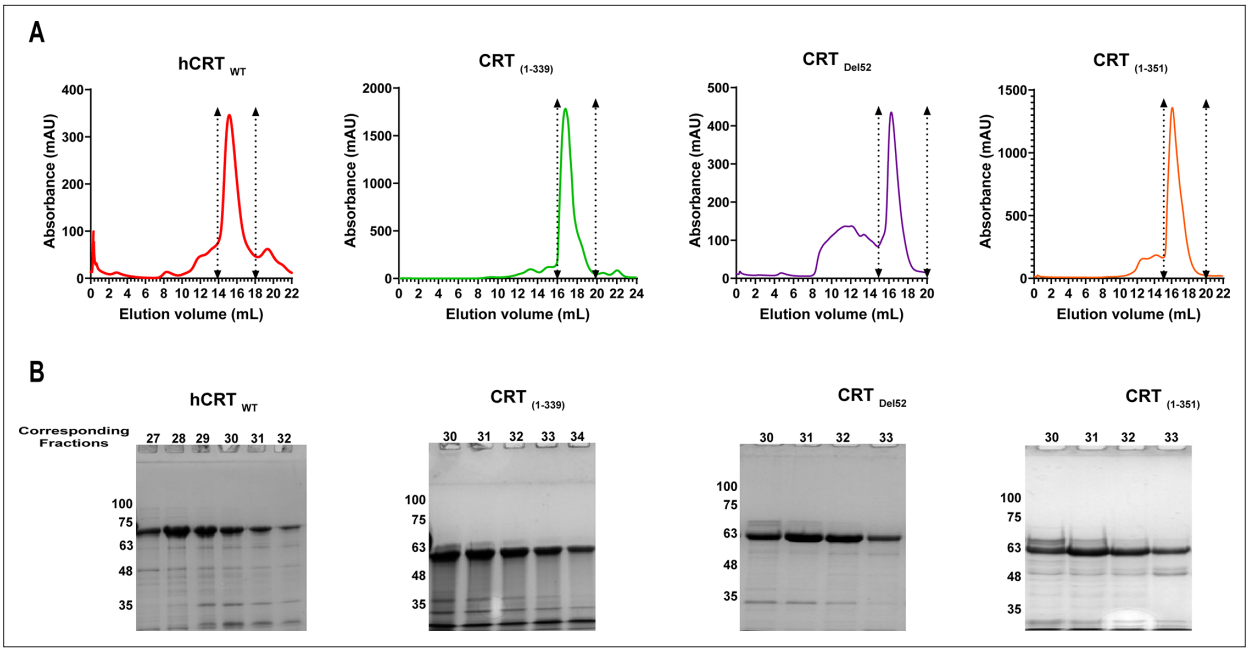


Figure 2. Purification of recombinant human wild-type CRT, CRT_{Del52}, and C-domain truncation mutants. (**A**) Representative chromatograms of recombinant GB1-and his-tagged human CRT_{WT} ($hCRT_{WT}$), CRT_{Del52}, and the C-domain truncation mutants $hCRT_{(1–351)}$ and $hCRT_{(1–339)}$ purified by gel exclusion chromatography after expression in *E. coli* and initial purification using a nickel resin. (**B**) Representative Coomassie blue-stained SDS-PAGE gels of fractions corresponding to the monomer peak (those contained within the region indicated by the double-headed arrows on the chromatogram) of purified proteins that were used for calcium-binding measurements. This figure has ***Figure 2—source data 1***, related to **A**, ***Figure 2—source data 2 and 3***, related to **B**.

The online version of this article includes the following source data for figure 2:

Source data 1. Chromatograms of purified recombinant CRT proteins.

Source data 2. Coomassie-stained SDS-PAGE gels.

Source data 3. Coomassie-stained SDS-PAGE gels.

CRT and also quantify ER and cytosolic calcium levels and calcium responsiveness in cells expressing wild-type CRT or CRT_{Del52}.

Results

MPN-linked CRT_{Del52} retained at least some low-affinity calcium-binding sites

Previous studies ***Wijeyesakere et al., 2011*** have implicated residues 340–351 of murine CRT, which are identical in wild-type human CRT and fully conserved with the 340–349 residues of CRT_{Del52}, to be involved in low-affinity calcium binding. Further truncation of the C-domain to the residue 339 ($mCRT_{1-339}$) led to the loss of calcium binding measured by ITC (***Wijeyesakere et al., 2011***). ***Figure 1*** shows a sequence alignment of murine CRT, human CRT, CRT_{Ins5}, and CRT_{Del52} proteins and indicates that the residues previously implicated in low-affinity calcium binding are also shared between wild-type CRT and CRT_{Del52}. Recombinant his- and GB1-tagged purified proteins were used to compare calcium binding by human CRT and its variants. Chromatograms for human wild-type CRT, CRT_{Del52}, $CRT_{(1–339)}$, and $CRT_{(1–351)}$ are shown in ***Figure 2A***. SDS-PAGE gels corresponding to the purified proteins are shown in ***Figure 2B***. Intact protein mass spectrometry for CRT_{Del52} indicated 35–42 amino acid truncations relative to the full protein sequence for different preparations, possibly from C-terminal protein degradation in *Escherichia coli*. The truncated proteins still include acidic residues 340–349 previously implicated in low-affinity calcium binding by murine CRT that are shared between wild-type and CRT_{Del52} (***Figure 1***).

CRT_{Ins5} was not purified in sufficient quantities needed for ITC experiments and was not further investigated in this study.

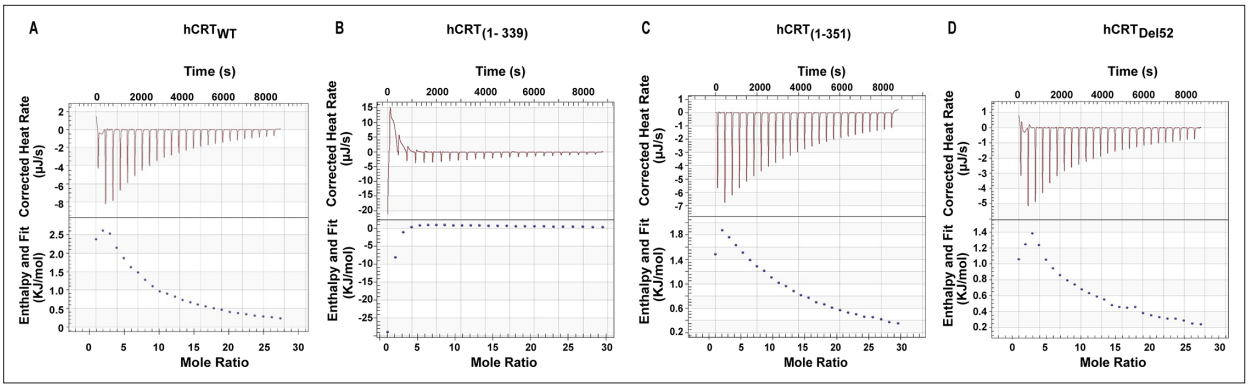


Figure 3. Calcium binding to the low-affinity sites of purified human CRT proteins. Low-affinity calcium binding by purified $hCRT_{WT}$, CRT_{Del52}, and the indicated truncation mutants was measured using isothermal titration calorimetry (ITC). (**A–D**) Representative isotherms and fitting curves of calcium binding to the low-affinity sites of the wild-type and mutant CRT proteins as indicated, measured using ITC. Prior to titration, the proteins were incubated with 50–100 µM $CaCl_2$ to block the high-affinity calcium-binding sites. At 37°C, 10 mM $CaCl_2$ was titrated against 100 µM protein. The heat change was measured for 25 injections, and the data were curve-fitted to calculate the dissociation constant, enthalpy, and binding stoichiometry using NanoAnalyze software. Data replicates and statistical analyses are specified in ***Table 1***. This figure has ***Figure 3—source data 1***, related to **A–D**.

The online version of this article includes the following source data for figure 3:

Source data 1. Isothermal titration calorimetry measurements of calcium binding to CRT proteins.

For the ITC measurements, calcium titrations were performed after pre-blocking the high-affinity calcium-binding sites with 50–100 µM $CaCl_2$. In a previous study (***Wijeyesakere et al., 2011***), we showed that at a starting calcium concentration of 0 mM and with $CaCl_2$ injections to a final concentration of 70–80 µM, the measured K_D value was 16.6 µM for calcium binding to wild-type murine CRT (which has ~95% sequence identity with human CRT), corresponding to the high-affinity site. On the other hand, at a starting calcium concentration of 50 µM and $CaCl_2$ injections (at 33 µM each) to a final concentration of 700–850 µM, the measured K_D value for calcium binding to wild-type murine CRT was 590 µM (corresponding to the low-affinity sites). We did not measure the high-affinity sites under the latter conditions (***Wijeyesakere et al., 2011***). In the present experiments, at starting $CaCl_2$ concentrations of 50–100 µM and 25 sequential 10 µL injections of 76 µM $CaCl_2$ to a final concentration of 1650–1700 µM, similar binding profiles and K_D values in the 400–1000 µM range were measured with wild-type human CRT, CRT_{Del52}, and the $CRT_{(1–351)}$ mutant (***Figure 3A, C, and D*** and ***Table 1***). However, consistent with previous studies with $mCRT_{(1–339)}$, endothermic calcium binding by human $CRT_{(1–339)}$ was of lower magnitude compared to other constructs, with a K_D value that was too low to be reliably fit, suggesting the loss of low-affinity calcium-binding sites in this mutant (***Figure 3B*** and ***Table 1***). There are exothermic peaks observed with human $CRT_{(1–339)}$ at the beginning of the calcium titration, which may be attributed to altered low-affinity sites retained within the mutant or reduced affinity of the high-affinity sites. We concluded that CRT_{Del52} retains at least some low-affinity calcium-binding sites that are measurable by ITC.

Table 1. Calorimetric data on measurement of calcium binding to the low-affinity binding site of recombinant purified CRT.

Recombinant CRT proteins/ isothermal calorimetric measurement	ΔH (k/mol)	n (mol)	Dissociation constant – K_D (µM)
CRT_{WT}	7.88±2.15	5.40±1.31	574.24±109.93
$CRT_{(1–351)}$	79.82±32.55	2.59±1.56	444.34±139.99
$CRT_{(1–339)}$	Too low to reliably fit		
CRT_{Del52}	3.89±1.36	7.73±1.81	938.82±275.89

Calorimetric data are represented as the mean ± SE. Data shown are averages from three to five independent replicates.

Similar ER calcium levels in CRT-KO HEK cells reconstituted with wild-type CRT or CRT_{Del52}

While the CRT_{Del52} mutant retains some ability to bind calcium (***Figure 3*** and ***Table 1***), the loss of the ER-retention KDEL sequence induced by the frameshift mutation, which results in the secretion of the protein from the ER (***Araki et al., 2016***; ***Chachoua et al., 2016***; ***Han et al., 2016***; ***Arshad and Cresswell, 2018***; ***Liu et al., 2020***; ***Masubuchi et al., 2020***; ***Venkatesan et al., 2021a***; ***Pecquet et al., 2023***) might be expected to cause ER calcium insufficiency in cells expressing CRT_{Del52} compared to wild-type CRT. We investigated ER calcium signals in CRT-KO HEK293T cells generated by CRISPR/Cas9 gene editing. A clonal KO line was generated and subsequently reconstituted with constructs encoding wild-type CRT, CRT_{Del52}, or CRT_{Del52} with a KDEL sequence added at the C-terminus ($CRT_{Del52\text{-}KDEL}$). Protein expression was assessed by immunoblotting with anti-CRT(N), which detects an N-domain epitope present in all CRT constructs, and anti-CRT(C-mut), which was specifically raised against the mutant CRT C-terminus (***Venkatesan et al., 2021a***). While the recognition with anti-CRT (N) was very weak in lysates of cells expressing CRT_{Del52}, which is secreted, $CRT_{Del52\text{-}KDEL}$ is readily detectable with both antibodies, consistent with prior studies demonstrating the contributions of the KDEL sequence to the ER retention of CRT and its mutants, including in human embryonic kidney (HEK) cells (***Arshad and Cresswell, 2018***; ***Sönnichsen et al., 1994***). Both wild-type CRT and $CRT_{Del52\text{-}KDEL}$ were reconstituted to higher levels than in the parental cells (***Figure 4A***, lanes 1 and 2 compared to 7–8 and 11–12).

The KO and reconstituted cells were further transfected with pCIS-GEM-CEPIA1er, which encodes a ratiometric ER calcium probe (***Suzuki et al., 2014***). Emission signals for calcium-bound (peak ~460 nm) and unbound (peak ~510 nm) probe were measured using flow cytometry in the Pacific Blue and AmCyan channels, respectively, following excitation with the 405 nm (violet) laser. Flow cytometric analysis was undertaken in a buffer containing 2 mM extracellular Ca^{2+} (***Figure 4B and C***). There was a significant decrease in basal free ER calcium, measured by the bound/unbound ratios in CRT-KO cells compared to the parental cells (***Figure 4D***, left panel). ER calcium levels were partially restored, although non-significantly, when the CRT-KO cells were reconstituted with wild-type CRT. CRT-KO cells reconstituted with CRT_{Del52} and $CRT_{Del52\text{-}KDEL}$ showed small but non-significant decreases in ER calcium levels compared to those reconstituted with wild-type CRT (***Figure 4D***, right panel). Changes to ER calcium levels in response to thapsigargin (Tg), a SERCA inhibitor, were similar in the parental vs. CRT-KO cells, and in the CRT-KO cells compared with those reconstituted with different CRT proteins (***Figure 4E***).

Spectrofluorimetry was used to verify the maintenance of ER calcium signals in the different HEK cell lines. Cells were again transfected with the pCIS-GEM-CEPIA1er probe and spectra were recorded in a buffer containing 2 mM Ca^{2+}, following excitation at 390 nm. Representative spectra are shown in ***Figure 5A***. Consistent with the flow cytometric measurements, there were no significant differences in the basal ER calcium levels between CRT-KO cells and those reconstituted with wild-type CRT or CRT_{Del52} (***Figure 5B***). There were also similar changes to ER calcium levels in response to Tg treatment in the CRT-KO cells compared to cells reconstituted with either wild-type CRT or CRT_{Del52} (***Figure 5C***).

Similar cytosolic calcium and SOCE signals in a CRT-KO megakaryocyte cell line reconstituted with wild-type CRT or CRT_{Del52}

MPN CRT mutations cause thrombopoietin-independent differentiation of megakaryocytes to platelets via the thrombopoietin receptor (MPL) (***Araki et al., 2016***; ***Chachoua et al., 2016***; ***Marty et al., 2016***; ***Li et al., 2018***; ***Masubuchi et al., 2020***). We, therefore, used a megakaryoblast cell line, MEG-01, to assess the role of CRT deficiency and the CRT_{Del52} mutant on basal cytosolic calcium levels and SERCA inhibition-induced calcium influx into the cytosol. As with the HEK cells (***Figure 4***), we created a stable CRT knockout clone of MEG-01 cells by CRISPR/Cas9 editing for cytosolic calcium measurements. The cells were subsequently reconstituted with wild-type CRT or CRT_{Del52}. Representative immunoblots are shown to demonstrate the successful knockout and reconstitution (***Figure 6A***). Wild-type CRT reconstitution in MEG-01 CRT-KO cells resulted in expression levels higher than those in the parental cells (***Figure 6A***, lanes 7 and 8 compared with lanes 1 and 2). In the presence of 2 mM Ca^{2+} in the media, we observed no significant differences in the basal cytosolic calcium levels or cyclopiazonic acid (CPA)-induced calcium release from ER in CRT-KO cells compared to the parental MEG-01 cells (***Figure 6C and D***). Additionally, no significant differences in basal cytosolic calcium were observed in CRT-KO cells compared to those reconstituted with wild-type CRT or CRT_{Del52} (***Figure 6E***).

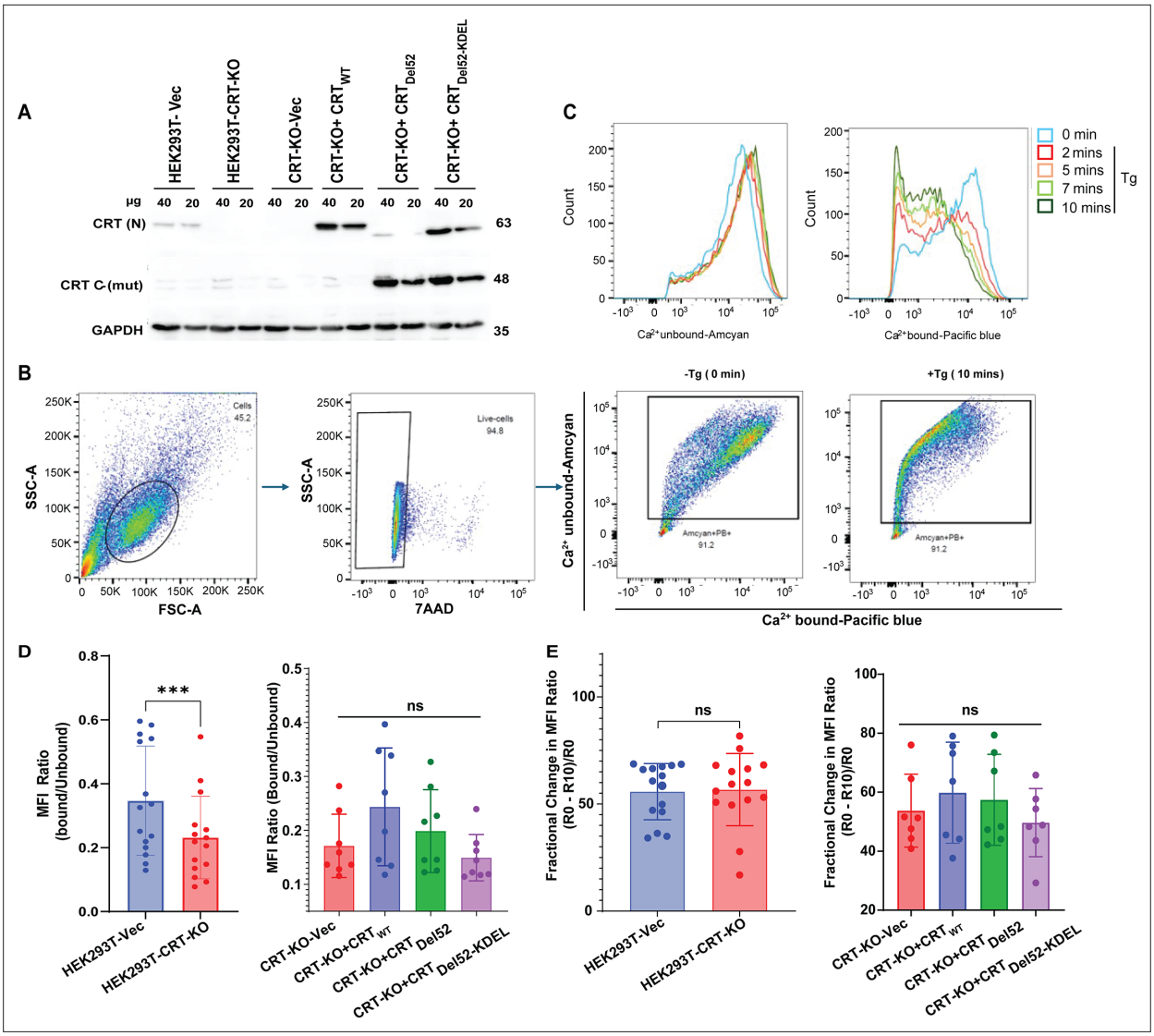


Figure 4. Flow cytometry-based endoplasmic reticulum (ER) calcium measurements indicate similar ER calcium levels in CRT-KO HEK293T cells and those reconstituted with wild-type CRT and CRT_{Del52}. (**A**) CRISPR-Cas9 editing of human embryonic kidney (HEK) cells using lentiviral constructs with calreticulin-targeting gRNA (CRT-KO) or empty vector (HEK-Vec). CRT-KO HEK cells were subsequently reconstituted with wild-type human CRT, CRT_{Del52}, or CRT_{Del52} with a C-terminal KDEL sequence as indicated. Representative blots showing expression levels of CRT in the indicated HEK cells. Cell lysates were subjected to SDS-PAGE followed by immunoblotting. Wild-type CRT, mutant CRT, and GAPDH were detected with anti-CRT (**N**), anti-CRT C-(mut), and anti-GAPDH antibodies, respectively. (**B**) Gating strategy for flow cytometry. HEK-Vec cells transiently transfected with the vector encoding the ratiometric GEM-CEPIA1er probe for 72 hr were used to assess ER calcium levels by flow cytometry based on the measurements of fluorescence emission signals for the Ca^{2+}-bound or unbound probe in the Pacific Blue and Amcyan channels, respectively, following excitation with the 405 nm (violet) laser. Transfected cells were gated based on forward (FSC-A) and side scatter (SSC-A), then on 7AAD-negative (live) cells, and further on the cells positive for the calcium-bound and unbound probe signals. Representative dot plots of changes in fluorescence intensities in response to treatment with thapsigargin (Tg), a SERCA inhibitor, before (0 min) or after (10 min) treatment, are shown. (**C**) Representative histograms showing changes to Ca^{2+}-bound and unbound signals at different time points following Tg treatment of cells. Mean fluorescence intensities (MFIs) for Ca^{2+}-bound and unbound signals were used to calculate the bound/unbound ratios at different time points. (**D and E**) The basal free ER calcium signals were measured as bound/unbound MFI ratios from the corresponding histograms of CRT-KO or HEK-Vec cells (**D**, left panel) or CRT-KO cells reconstituted with the indicated CRT constructs (D, right panel). The fractional changes in ER calcium signals in response to Tg were measured in the indicated cells (**E**). The fractional change ratios were calculated as $(R_0–R_{10}/R_0)\times100$. Statistical significance was determined using GraphPad Prism and based on paired t-tests (left panels of D and E) or repeated-measures one-way ANOVAs with Tukey's test (right panels of **D and E**). ns, not significant; ***p-value≤0.001. All measurements were undertaken in the presence of 2 mM extracellular Ca^{2+}. Data shown in **D and E** are based on 7–15 independent experiments as indicated by the individual data points within the graphs. GAPDH, glyceraldehyde-3-phosphate dehydrogenase; SDS-PAGE, sodium dodecyl sulfate-polyacrylamide gel electrophoresis. This figure has ***Figure 4—source data 1 and 2***, related to **A**, ***Figure 4—source data 3***, related to **D–E**.

Figure 4 continued on next page

Figure 4 continued

The online version of this article includes the following source data for figure 4:

Source data 1. Immunoblots of CRT expression in HEK293T cells.

Source data 2. Immunoblots of CRT expression in HEK293T cells.

Source data 3. Flow cytometry-based endoplasmic reticulum (ER) calcium measurements in HEK293T cells.

Furthermore, cytosolic calcium levels in CRT-KO and the two reconstituted cell lines were not statistically different following CPA treatments.

CALR mutations are generally found in BCR-ABL1-negative MPN (***Klampfl et al., 2013***; ***Nangalia et al., 2013***), whereas MEG-01 cells have the BCR-ABL1 translocation (***Ogura et al., 1985***), which induces constitutive tyrosine kinase activity. This could influence intracellular calcium homeostasis (***Cabanas et al., 2018***). To eliminate possible effects of BCR-ABL1 expression on the measured responses (***Figure 6***), cytosolic calcium signals in the various MEG-01 cell lines were compared with and without treatment of cells with the tyrosine kinase inhibitor, Imatinib. We initially verified the effect of Imatinib on MEG-01 cells by assessing the expression of STAT5 and the formation of phospho-STAT5 using immunoblots. These analyses showed significantly reduced or abrogated phospho-STAT5 expression upon Imatinib treatment (***Figure 6—figure supplement 1***). Similar to the findings in the absence of Imatinib (***Figure 6***, left panel), there were no significant differences in the basal cytosolic calcium levels in Imatinib-treated CRT-KO cells compared to those reconstituted with wild-type CRT and CRT_{Del52} (***Figure 6—figure supplement 2***, left panel). Likewise, CPA-induced calcium release from ER was generally similar in CRT-KO cells compared to cells reconstituted with wild-type CRT or CRT_{Del52} both in imatinib-treated and untreated cells (***Figure 6—figure supplement 2***, middle and right panels).

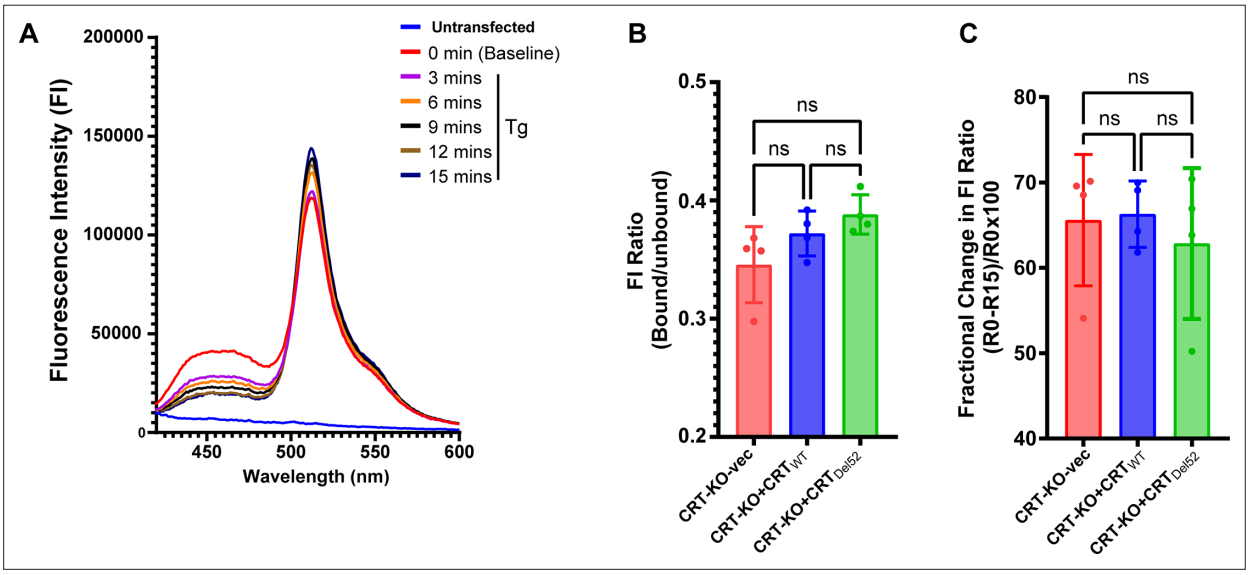


Figure 5. Fluorimetry-based endoplasmic reticulum (ER) calcium measurements indicate similar ER calcium levels in CRT-KO HEK293T cells and those reconstituted with wild-type CRT and CRT_{Del52}. Human embryonic kidney (HEK) cells transiently transfected with a vector encoding the ratiometric GEM-CEPIA1er probe for 72 hr were used to assess ER calcium levels in the presence of 2 mM extracellular Ca^{2+}. Fluorescence emission spectra were recorded following excitation at 390 nm. (**A**) Representative emission spectra show changes to Ca^{2+}-bound (~460 nm) and unbound (~510 nm) peaks at different time points following Tg treatment of cells. The spectrum in blue was obtained with untransfected HEK cells. (**B**) Basal Ca^{2+}-bound (~460 nm)/unbound (~510 nm) fluorescence intensity (FI) ratios were calculated for the indicated HEK cell lines before Tg addition. (**C**) The fractional changes to the bound (~460 nm)/unbound (~510 nm) fluorescence intensity ratios at 15 min relative to baseline were calculated as $(R_0–R_{15}/R_0)\times100$. Statistical significance was determined by repeated-measures one-way ANOVAs with Tukey's test using GraphPad Prism. Data shown are based on four independent experiments, indicated by the individual data points within the graphs. ns, not significant. This figure has ***Figure 5—source data 1***, related to **B and C**.

The online version of this article includes the following source data for figure 5:

Source data 1. Spectrofluorimetric endoplasmic reticulum (ER) calcium measurements in HEK293T cells.

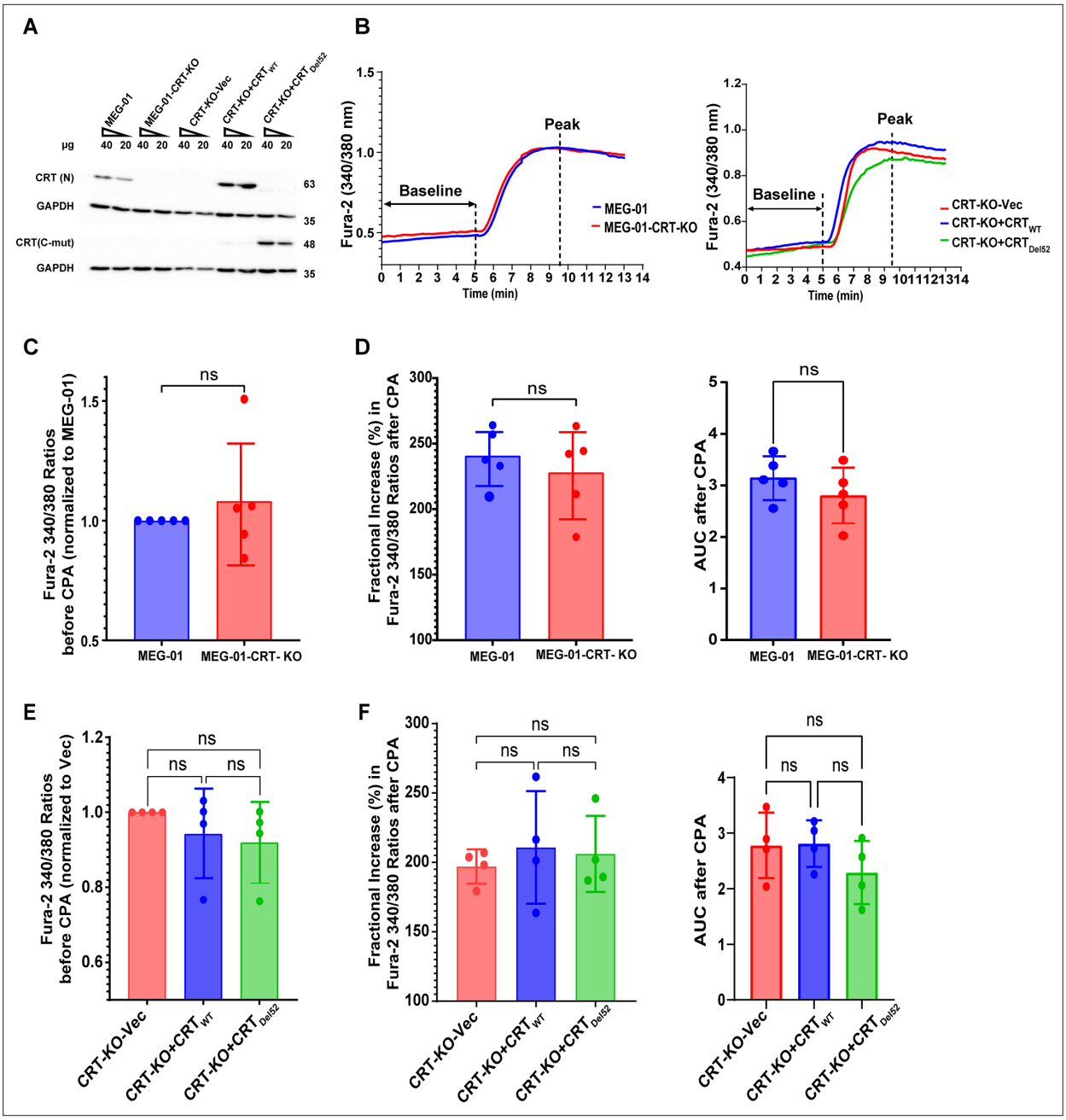


Figure 6. Calcium imaging studies indicate similar cytosolic calcium levels in the megakaryoblastic (MEG-01) cells with CRT-KO and those reconstituted with wild-type CRT or CRT_{Del52}. (**A**) CRISPR-Cas9 editing of MEG-01 cells using lentiviral constructs encoding calreticulin-targeting gRNA (CRT-KO). CRT-KO MEG-01 cells were subsequently reconstituted with viral constructs encoding wild-type human CRT or CRT_{Del52} or transduced with empty vector (Vec) as indicated in the figure panels. Representative immunoblots of CRT expression in the indicated cells detected by the anti-CRT(N) and anti-CRT(C-mut) antibodies. (**B–F**) Cells in 2 mM extracellular Ca^{2+} were loaded with the Fura-2/AM dye. Following excitation at 340 or 380 nm and recordings of emission at 510 nm, the emission ratios (340/380) are calculated. (**B**) Representative calcium imaging data from indicated cells in the presence of 2 mM extracellular Ca^{2+} and following ER calcium depletion with SERCA inhibitor, cyclopiazonic acid (CPA). (**C and E**) Basal cytosolic calcium levels are plotted as the mean 340/380 ratios. Data were normalized relative to the MEG-01 signals. (**D and F**) Mean fractional changes to cytosolic calcium levels calculated as $(R_{peak}–R_{baseline}/R_{baseline})\times100$ and total calcium release determined as the area under the curve (AUC) are plotted. Data shown in C–F are based on four or five independent experiments with measurements averaged from 50 to 100 cells per experiment. Statistical analysis was performed using paired t-tests (**C and D**) or repeated-measures one-way ANOVAs with Tukey's test (**E and F**). Statistical significance was determined based on p-value≤0.05 using GraphPad Prism. ns, not significant. This figure has ***Figure 6—source data 1 and 2*** related to **A**, ***Figure 6—source data 3***, related to **C–D**, and ***Figure 6—source data 4***, related to **E–F**. This figure has two figure supplements: ***Figure 6—figure supplements 1 and 2***.

The online version of this article includes the following source data and figure supplement(s) for figure 6:

Figure 6 continued on next page

Figure 6 continued

Source data 1. Immunoblots of CRT expression in MEG-01 cells.

Source data 2. Immunoblots of CRT expression in MEG-01 cells.

Source data 3. Cytosolic calcium measurements in MEG-01 parental and CRT-KO cells.

Source data 4. Cytosolic calcium measurements in CRT-KO cells and those reconstituted with wild-type CRT and CRT_{Del52}.

Figure supplement 1. Imatinib treatment reduces p-STAT5 levels.

Figure supplement 1—source data 1. Immunoblots of STAT5 and phospho-STAT5 in cells with or without imatinib treatment.

Figure supplement 1—source data 2. Immunoblots of STAT5 and phospho-STAT5 in cells with or without imatinib treatment.

Figure supplement 2. Calcium imaging studies indicate similar cytosolic calcium levels in MEG-01 CRT-KO cells, and those reconstituted with wild-type CRT or CRT_{Del52} both with and without imatinib treatment.

Figure supplement 2—source data 1. Cytosolic calcium measurements with and without imatinib treatment.

SOCE is an important process for restoring ER calcium and maintaining intracellular calcium levels. In contrast to cytosolic calcium signals in the presence of 2 mM Ca^{2+} in the media, in calcium-free saline, CRT-KO cells exhibited a small but significant increase in basal cytosolic calcium levels relative to the parental cells (***Figure 7A***, left panel, and ***Figure 7B***). Upon ER calcium depletion with CPA, the mean fractional increase in the cytosolic calcium measured in the Ca^{2+}-free saline did not differ significantly in parental cells vs. CRT-KO cells. The areas under the curve were also not different for the two cell lines (***Figure 7A and C***). However, consistent with the higher basal cytosolic calcium measured in CRT-KO cells in calcium-free saline, the measured SOCE signal (following the addition of 2 mM Ca^{2+} and CPA) was significantly reduced in CRT-KO cells compared to parental cells (***Figure 7D***). Reconstitution of the CRT-KO cells with either wild-type CRT or CRT_{Del52} tended to reduce basal cytosolic calcium and induce SOCE (***Figure 7A***, right panel, ***Figure 7E and G***), but both trends were non-significant compared to CRT-KO cells. Importantly, there were no significant differences between the wild-type CRT and CRT_{Del52} reconstituted cells, in either their basal or CPA-induced cytosolic calcium signals or in SOCE (***Figure 7E–G***). In calcium-free saline, cytosolic calcium signals and SOCE induction were generally similar in CRT-KO cells as in the wild-type CRT and CRT_{Del52} reconstituted cells, both in the presence and absence of imatinib (***Figure 7—figure supplement 1***).

CRT deficiency induced numerous transcriptional changes to genes within the calcium signaling pathway

As noted in ***Figures 4 and 7***, some of the measured differences between CRT-KO and parental cells are not fully reversed by reconstitution with wild-type CRT, although the trends are maintained. We predicted that there may be other indirect effects of CRT-KO and reconstitution that affect cellular calcium levels and calcium signaling that could explain some of these measured differences. As proof of concept, we undertook bulk RNA sequencing to determine differential gene expression in MEG-01 parental vs. CRT-KO cells. There were 3078 upregulated and 1790 downregulated genes. The volcano plot and heatmap show identified genes that were differentially expressed in CRT-KO MEG-01 compared to parental cells (***Figure 8A***). Based on pathway analysis, numerous genes involved in cellular calcium signaling were identified. Of specific note is the upregulation of GRP94 encoded by the *HSP90B1* gene, BiP encoded by the *HSPA5* gene, and PDIA6 encoded by the *PDIA6* gene, which are known to have low-affinity calcium-binding sites (***Lièvremont et al., 1997***; ***Macer and Koch, 1988***; ***Biswas et al., 2007***; ***Marzec et al., 2012***; ***Okumura et al., 2021***; ***Figure 8A and B***). Other studies have reported similar upregulation of these genes in CRT-KO (***Tang et al., 2025***), as well as in heterozygous CRT_{Del52} knock-in cells (***Figure 8C***; ***Foßelteder et al., 2023***). Upregulation of these proteins may serve a compensatory role in buffering calcium in CRT-KO cells. Additionally, PDIA3, which is shown to regulate the activities of stromal interaction molecule 1 (STIM1) (***Prins et al., 2011***) and sarcoplasmic reticulum/ER Ca^{2+} ATPase (SERCA2b) (***Li and Camacho, 2004***), was consistently upregulated in all the studies.

We further used real-time polymerase chain reaction (PCR) with target gene primers (***Supplementary file 1B***) to validate the expression of the key ER-resident proteins identified from the RNA sequencing data which have roles in calcium binding and regulation of ER calcium homeostasis. Consistent with the RNA sequencing data, the expression of *HSPA5*, *HSP90B1*, *PDIA6*, and *PDIA3* mRNA

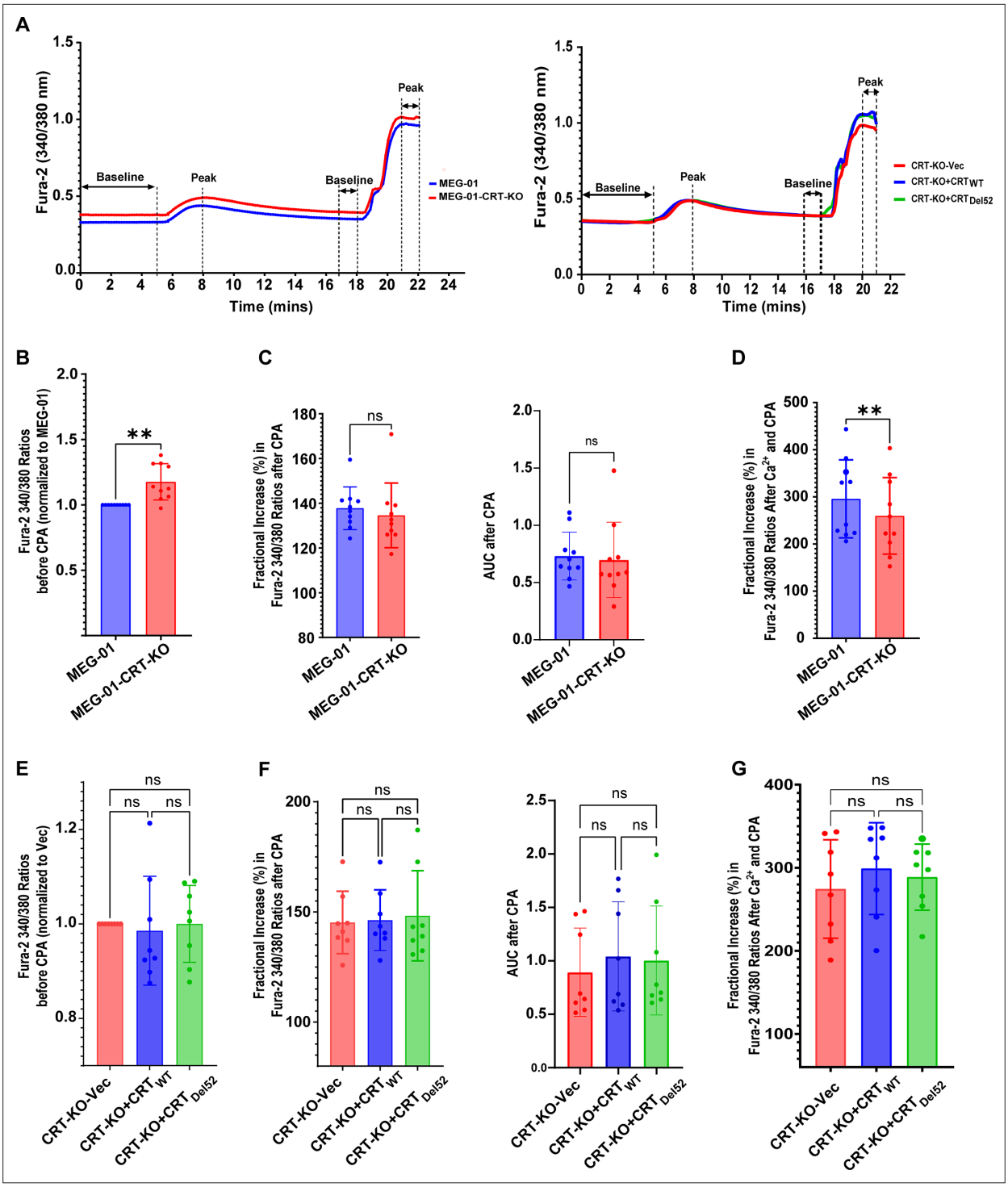


Figure 7. Calcium imaging studies indicate similar cytosolic calcium levels and store-operated calcium entry (SOCE) in MEG-01 cells with CRT-KO and those reconstituted with wild-type CRT or CRT_{Del52}. Cells were loaded with Fura-2/AM dye. Following excitation at 340 or 380 nm and recordings of emission at 510 nm, the emission ratios (340/380) were calculated. (**A**) Representative calcium imaging data from cells in the absence of extracellular calcium, followed by the addition of cyclopiazonic acid (CPA), and subsequent addition of extracellular calcium and CPA as indicated. (**B and E**) Basal cytosolic calcium levels are plotted as the mean 340/380 ratios prior to CPA addition. Data are normalized relative to the signals of cells transduced with empty vector (Vec). (**C and F**) Fractional changes to cytosolic calcium calculated as $(R_{peak}–R_{baseline}/ R_{baseline})\times100$ (left panel) and total calcium release measured as the area under the curve (AUC) (right panel) are plotted for the indicated cells, following ER calcium depletion with CPA. (**D and G**) Fractional changes to cytosolic calcium following CPA and extracellular calcium additions (2 mM) are calculated as $(R_{peak}–R_{baseline}/R_{baseline})\times100$, where $R_{baseline}$ and R_{peak} were measured over 1 min intervals. Data shown are based on 8–10 independent experiments, and an average of over 20–100 cells

Figure 7 continued on next page

Figure 7 continued

in each experiment. Comparisons were performed by paired t-test (panels B–D) and one-way ANOVA (panels **E–G**) using GraphPad Prism. Statistical significance is based on a p-value≤0.05. ns, not significant, **p≤0.01. This figure has ***Figure 7—source data 1***, related to **B–D**, ***Figure 7—source data 2***, related to **E–G**. This figure has one supplement, ***Figure 7—figure supplement 1***.

The online version of this article includes the following source data and figure supplement(s) for figure 7:

Source data 1. Cytosolic calcium measurements and store-operated calcium entry (SOCE) in parental and CRT-KO cells.

Source data 2. Cytosolic calcium measurements and store-operated calcium entry (SOCE) in CRT-KO cells and those reconstituted with wild-type CRT and CRT_{Del52}.

Figure supplement 1. Calcium imaging studies indicate similar cytosolic calcium levels and store-operated calcium entry (SOCE) in MEG-01 CRT-KO cells and those reconstituted with wild-type CRT or CRT_{Del52} both with and without imatinib treatment.

Figure supplement 1—source data 1. Cytosolic calcium measurements and store-operated calcium entry (SOCE) with and without imatinib treatment.

transcripts was significantly increased in CRT-KO MEG-01 compared to parental cells. Reconstitution of CRT-KO cells with wild-type CRT but not CRT_{Del52} showed a significant decrease in the expression of *HSPA5, HSP90B1, PDIA6*, and *PDIA3* (***Figure 8D–G***). Protein levels of BiP, GRP94, PDIA6, and PDIA3 were also assessed in the indicated cells by immunoblots using specific antibodies. Representative immunoblots show increased expression of BiP (***Figure 8D***, right panel), GRP94 (***Figure 8E***, right panel), PDIA6 (***Figure 8F***, right panel), and PDIA3 (***Figure 8G***, right panel) in CRT-KO cells compared to parental MEG-01 cells, as well as increased expression in CRT-KO-Vec cells compared to CRT-KO cells reconstituted with wild-type CRT. The effects of CRT_{Del52} in reducing expression were generally less robust than wild-type CRT.

Discussion

Calreticulin is a ubiquitously expressed ER luminal calcium-binding chaperone, with a role in ER calcium storage (***Venkatesan et al., 2021b***; ***Michalak, 2024***). A number of prior studies have examined the effects of CRT deficiency and overexpression upon cytosolic and ER calcium signals and SOCE (***Arnaudeau et al., 2002***; ***Bastianutto et al., 1995***; ***Mery et al., 1996***; ***Nakamura et al., 2001***). CRT deficiency in mouse fibroblasts did not affect free ER calcium levels relative to wild-type cells (***Nakamura et al., 2001***). Previous studies using dye-based assays reported impaired calcium binding by the MPN-associated CRT_{Del52} mutant (***Ibarra et al., 2022***). Yet, direct and more quantitative analyses of its calcium-binding properties have been lacking. In this study, we investigated low-affinity calcium binding by wild-type human CRT, CRT_{Del52}, and the truncation mutants $CRT_{(1–351)}$ and $CRT_{(1–339)}$ using ITC (***Figure 3*** and ***Table 1***). Our studies show that wild-type CRT, CRT_{Del52}, and $CRT_{(1–351)}$ retain low-affinity calcium-binding sites, exhibiting average K_D values of 574.24, 938.82, and 444.34 μM, respectively. On the other hand, low-affinity calcium binding by $CRT_{(1–339)}$ could not be reliably fit. This is the first quantitative characterization of the low-affinity calcium-binding profiles of wild-type human CRT, CRT_{Del52}, and functionally informative truncation mutants.

Although CRT_{Del52} retains at least partial low-affinity calcium-binding capability, loss of its KDEL retention sequence (***Figure 1***) could still disrupt ER calcium storage and signaling. Interestingly, the cellular assays reveal that ER and cytosolic calcium levels, as well as SOCE, are similar between CRT-KO cells and those reconstituted with either wild-type CRT or CRT_{Del52} (***Figures 4–7***). One study has reported decreased ER calcium levels in a human osteosarcoma cell line transiently transfected to overexpress a CRT type I mutant, compared to those overexpressing wild-type CRT or a type II mutant, which was linked to unfolded protein response induction in type I mutant-expressing cells (***Ibarra et al., 2022***). The same study suggested the contributions of the P- and C-domains of wild-type CRT in restoring ER calcium levels in cells expressing CRT_{Del52} (***Ibarra et al., 2022***). The conditions of those experiments differ from the studies described in our study, which uses a CRT-KO background with wild-type CRT or CRT_{Del52} reconstitutions to simulate homozygous MPN type I CALR mutations. Achieving endogenous expression levels of wild-type CRT is a limitation of our study, as in many other studies examining the effects of CRT on cellular calcium signaling. Despite this, our findings are consistent with the theoretical prediction that any excess free ER calcium generated in cells lacking CRT or sufficient ER calcium-binding sites would rapidly diffuse out of the ER and be pumped out of the cell.

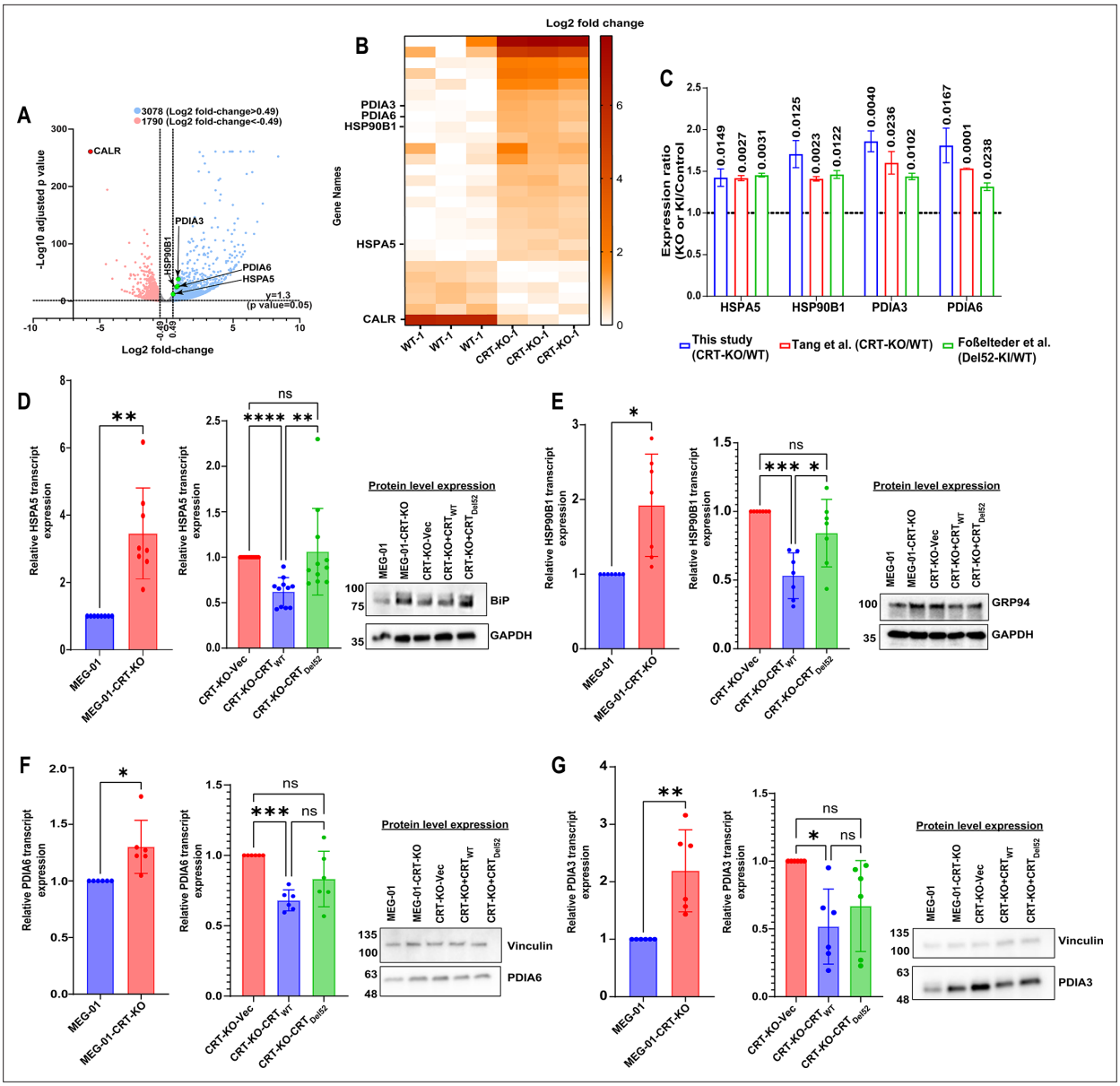


Figure 8. Transcriptional changes to the expression of genes encoding endoplasmic reticulum (ER) calcium-binding/regulating proteins in CRT-KO MEG-01 cells. (**A**) RNA sequencing analysis was used to identify differentially expressed genes in MEG-01 CRT-KO cells in comparison to parental MEG-01 cells. Volcano plot shows significantly upregulated (blue) and downregulated (red) genes identified by RNA sequencing. Genes related to ER calcium binding and homeostasis have been highlighted and labeled. The differentially expressed genes were selected as those with a $\log_2$ fold-change of <−0.49 or >0.49 and p-values <0.05. (**B**) Heatmap shows the differential expression of genes encoding ER-resident calcium-binding proteins or ER calcium regulators that were identified by RNA sequencing in CRT-KO Meg-01 cells compared to parental cells (n=3 biological replicates). (**C**) Comparison of expression ratio of *HSPA5*, *HSP90B1*, *PDIA3*, and *PDIA6* in CRT-KO MEG-01 cells (this study) or murine lung cancer cells (***Tang et al., 2025***), heterozygous CRT_{Del52} knock-in (Del52-KI) cells (***Foßelteder et al., 2023***) normalized to their expression in respective control cell lines expressing wild-type CRT. The normalized expression of various genes identified in each dataset was calculated as a ratio of expression in CRT-KO, CRT_{Del52} knock-in, or CRT_{Del52} cells relative to the expression in wild-type CRT-expressing cells. Multiple unpaired t-tests were used to determine statistical significance with the Benjamini-Hochberg FDR correction (p-adjusted)<0.05. (**D–G**) Left and middle panels: Relative expression of mRNA transcripts of *HSPA5* (n=8–11), *HSP90B1* (n=7), *PDIA6* (n=6), and *PDIA3* (n=6) genes in the indicated MEG-01 cells determined by RT-qPCR using specific gene primers. Relative gene expression was calculated by normalizing the target gene's cycle threshold (Ct) to a single or multiple endogenous controls (ACTB, GAPDH, and HPRT1), which was used for comparison across different cell lines as indicated. Data show 6–11 independent runs with duplicate measurements for each run. Student's t-test was used to determine the statistical significance between two groups while multiple group comparison was performed by one-way ANOVA using GraphPad Prism. Statistical significance is based on a p-value≤0.05. ns, not significant, *p≤0.05, **p≤0.01, ***p≤0.001, ****p≤0.0001. Right panels: Representative immunoblots of BiP, GRP94, PDIA6, and PDIA3 expression in the indicated cells detected by specific antibodies. This figure

Figure 8 continued on next page

Figure 8 continued

has ***Figure 8—source data 1***, related to **C**, ***Figure 8—source data 2***, related to **D–G** (left panels), and ***Figure 8—source data 3 and 4***, related to **D–G** (right panels).

The online version of this article includes the following source data for figure 8:

Source data 1. Comparison of expression ratio of *HSPA5, HSP90B1, PDIA3*, and *PDIA6.*

Source data 2. Relative expression of mRNA transcripts of *HSPA5*, *HSP90B1*, *PDIA6,* and *PDIA3* genes.

Source data 3. Immunoblots of BiP, GRP94, PDIA6, and PDIA3 expression.

Source data 4. Immunoblots of BiP, GRP94, PDIA6, and PDIA3 expression.

Related to cytosolic calcium levels and SOCE activation, consistent with our findings (***Figure 7G***, ***Figure 7—figure supplement 1***), a previous study found no differences in cytosolic calcium levels or SOCE induction in myeloid progenitor 32D cells expressing wild-type CRT and CRT_{Del52} both under conditions of cytokine deprivation and thrombopoietin stimulation (***Bhuria et al., 2024***). On the other hand, studies with cultured megakaryocytes from MPN patients with *CALR* mutations have reported cytosolic calcium abnormalities compared to healthy control cells (***Di Buduo et al., 2020***; ***Pietra et al., 2016***). In one study, cultured megakaryocytes from patients with type I but not type II *CALR* mutations were found to have high cytosolic calcium and SOCE activation in cultured megakaryocytes (***Pietra et al., 2016***). In another study, a larger number of cultured megakaryocytes from MPN patients with type I or type II *CALR* mutations displayed spontaneous cytosolic calcium spikes and reduced CRT interactions with stromal interaction molecule I (STIM-1) (reflective of SOCE) compared with megakaryocytes from healthy donors or patients with the JAK2V617F mutation (***Di Buduo et al., 2020***). Thus, there are differences in the findings of the two studies with primary cultured megakaryocytes, the first of which reported increased SOCE activation in cultured megakaryocytes from patients with type I but not type II *CALR* mutations, and the second of which reported increased frequency of cytosolic calcium spikes and reduced STIM-1-CRT binding in cultured megakaryocytes from patients with both type I and type II *CALR* mutations (***Pietra et al., 2016***; ***Di Buduo et al., 2020***). In the absence of engineered controls, sample-to-sample heterogeneities in primary cells make it difficult to attribute any measured differences to direct rather than indirect effects of CRT mutations on cellular calcium signaling.

We found that CRT-KO HEK cells displayed lower ER calcium compared with the parental HEK cells (***Figure 4D***, left panel) and also that CRT-KO MEG-01 cells displayed increased cytosolic calcium in the absence of extracellular calcium (***Figure 7B***). However, reconstitutions with wild-type CRT did not reverse these effects (***Figure 4D***, right panel, and ***Figure 7E***). Transcriptomic analysis identified significant alterations in the expression of genes related to calcium storage and signaling between parental and CRT-KO MEG-01 cells (***Figure 8***). These changes highlight adaptive or compensatory pathways induced by CRT-KO and emphasize that, when comparing wild-type and CRT-KO cell lines for subcellular calcium levels or responses to SERCA inhibitors, the measured effects might not be based solely on the abilities of CRT to maintain ER and cytosolic Ca^{2+} levels via its calcium binding, storage, and buffering capacity. Rather, many other compensatory cellular changes could affect subcellular calcium levels and signaling. In this study, various ER proteins with known calcium-binding activities were found to be upregulated in CRT-KO cells (***Figure 8A and B***). GRP94 (***Macer and Koch, 1988***; ***Biswas et al., 2007***; ***Marzec et al., 2012***), BiP (***Lièvremont et al., 1997*** and our unpublished findings), and PDIA6 (***Okumura et al., 2021***) are each known to contain low-affinity calcium-binding sites. CRT-KO cells have significantly induced expression of the genes encoding these proteins. Wild-type CRT reconstitution into the CRT-KO cells significantly reduced the expression of these ER proteins, whereas CRT_{Del52} reconstitution only partly and non-significantly reduced the expression of *HSP90B1* and *PDIA6* and did not reduce the expression of *HSPA5* (***Figure 8D–F***). GRP94, BiP, and PDIA6 have functions in ER protein folding and quality control (***Hendershot et al., 2024***; ***Okumura et al., 2021***). Related to the mechanisms of induction of calcium-binding proteins, it is known that CRT_{Del52} has impaired chaperone activity toward its substrates compared with wild-type CRT (***Arshad and Cresswell, 2018***; ***Schürch et al., 2022***; ***Kaur et al., 2025***). This could account for some of the measured differences between wild-type CRT and CRT_{Del52} in altering the expression of the ER calcium-binding proteins that also function as chaperones and folding factors. However, the induction of GRP94, BiP, and PDIA6 in knock-in cells with heterozygous expression of wild-type CRT and CRT_{Del52} (***Foßelteder et al., 2023***), where the

wild-type CRT appears sufficient for protein folding activities (***Kaur et al., 2025***; ***Schürch et al., 2022***), points to compensatory effects relevant to calcium signaling. Regardless of the precise mechanisms relevant to the induction of the calcium-binding proteins, their combined expression, despite protein compositional differences between the KO and reconstituted cells, appears sufficient to maintain ER calcium levels (***Figure 4D***, right panel), calcium release from the ER (***Figure 4E***, right panel, and ***Figure 6F***), and cytosolic calcium levels (***Figure 6E***).

PDIA3 (ERp57) forms a complex with CRT and interacts with and regulates the activities of the ubiquitously expressed SERCA2b (***Li and Camacho, 2004***). Its expression is also induced by the CRT-KO and suppressed by wild-type CRT expression but non-significantly by CRT_{Del52} expression. Altered SERCA2b activity could also affect basal ER calcium levels, contributing to similarities between CRT-KO and wild-type CRT or CRT_{Del52} reconstituted cells.

Collectively, our findings reveal that CRT_{Del52} retains some ability to bind calcium at low-affinity sites. CRT-KO cells reconstituted with wild-type or CRT_{Del52} have comparable ER and cytosolic calcium levels and SOCE. CRT-KO induces broad changes in ER calcium-binding protein expression as well as in the expression of ERp57. Overall, we can conclude that a number of factors that contribute to the maintenance of ER calcium levels and regulation of calcium transport into the ER are altered in CRT-KO cells. Thus, any disease-related changes in calcium signaling and homeostasis are likely multifactorial, encompassing transcriptional regulation and altered expression of critical mediators of calcium storage, transport, and signaling pathways. These studies provide a more nuanced understanding of CRT's role in cellular calcium signaling and may inform future therapeutic strategies targeting calcium signaling pathways in hematological malignancies.

Materials and methods

Key resources table

Reagent type (species) or resource	Designation	Source or reference	Identifiers	Additional information
Strain, strain background (*Escherichia coli*)	Origami B(DE3)	Sigma-Aldrich	Ref 70836-M	Chemically competent
Cell line (human)	MEG-01	ATCC	RRID:CVCL_0425	This cell line was authenticated by Labcorp using STR genotyping
Cell line (human)	HEK293T	ATCC	RRID:CVCL_0063	This cell line was authenticated by Labcorp using STR genotyping
Antibody	Anti-CRT (N) (rabbit monoclonal)	Cell Signaling Technology	CST #12238;RRID:AB_2688013	1:5000
Antibody	Anti-CRT (C-mut)	PMCID:PMC8085772		1:10,000
Antibody	Anti-GRP78/BiP (rabbit polyclonal)	Proteintech	11587–1-AP;RRID:AB_2119855	1:10,000
Antibody	Anti-GRP94 (rabbit polyclonal)	Proteintech	14700–1-AP;RRID:AB_2233347	1:10,000
Antibody	Anti-ERp57 or PDIA3 (rabbit polyclonal)	Proteintech	15967–1-AP;RRID:AB_2236784	1:10,000
Antibody	Anti-PDIA6 (rabbit polyclonal)	Proteintech	18233–1-AP;RRID:AB_10805765	1:20,000
Antibody	Anti-STAT5 (rabbit monoclonal)	Cell Signaling Technology	CST #94205;RRID:AB_2737403	1:1000
Antibody	Anti-phospho-STAT5 (rabbit monoclonal)	Cell Signaling Technology	CST # 9359;RRID:AB_823649	1:1000
Antibody	Anti-vinculin	Cell Signaling Technology	CST 13901;RRID:AB_2728768	1:20,000
Antibody	Anti-GAPDH	Cell Signaling Technology	CST 2118;RRID:AB_561053	1:20,000
Recombinant DNA reagent	pCIS-GEM-CEPIA1er (plasmid)	Addgene	RRID:Addgene_58217	
Recombinant DNA reagent	psPAX2 (plasmid)	Addgene	RRID:Addgene_12260	
Recombinant DNA reagent	pMD2.G	Addgene	RRID:Addgene_12259	
Recombinant DNA reagent	pMSCV (plasmid)	Addgene	RRID:Addgene 75085	
recombinant DNA reagent	ZsGreen1 (pLVX-IRES-Puro)	Addgene	RRID:Addgene_180278	
Recombinant DNA reagent	pLentiCRISPRv2-BLAST (pLB)	Addgene	RRID:Addgene_98293	
Recombinant DNA reagent	pSIP-$CALR_{WT}$ (plasmid)	This paper		Wild-type calreticulin ($CALR_{WT}$) cDNA cloned in pSIP-*ZsGreen* (pLVX-SFFV-IRES-Puro) vector at EcoRI and NotI sites

Continued on next page

Continued

Reagent type (species) or resource	Designation	Source or reference	Identifiers	Additional information
Recombinant DNA reagent	pSIP-*CALR*$_{Del52}$ (plasmid)	This paper		Mutant calreticulin (*CALR*$_{Del52}$) cDNA cloned in pSIP-ZsGreen (pLVX-SFFV-IRES-Puro) vector at EcoRI and NotI sites
Recombinant DNA reagent	pSIP-*CALR*$_{Del52+KDEL}$ (plasmid)	This paper		Mutant calreticulin+KDEL (*CALR*$_{Del52+KDEL}$) cDNA cloned in pSIP-ZsGreen (pLVX-SFFV-IRES-Puro) vector at EcoRI and NotI sites
Recombinant DNA reagent	pGB1-*CALR*$_{WT}$ (plasmid)	This paper		B1 domain of streptococcal protein G (GB1) (***Huth et al., 1997***) and hexa-histidine tag using the pGB1 vector via ligation-independent cloning, as described earlier (***Del Cid et al., 2010***; ***DelProposto et al., 2009***)
Recombinant DNA reagent	pGB1-*CALR*$_{(1-351)}$ (plasmid)	This paper		B1 domain of streptococcal protein G (GB1) (***Huth et al., 1997***) and hexa-histidine tag using the pGB1 vector via ligation-independent cloning, as described earlier (***Del Cid et al., 2010***; ***DelProposto et al., 2009***) with quickchange site mutagenesis
Recombinant DNA reagent	pGB1-*CALR*$_{(1-339)}$ (plasmid)	This paper		B1 domain of streptococcal protein G (GB1) (***Huth et al., 1997***) and hexa-histidine tag using the pGB1 vector via ligation-independent cloning, as described earlier (***Del Cid et al., 2010***; ***DelProposto et al., 2009***) with quickchange site mutagenesis
Sequence-based reagent	ACTB (Primer)	Real-time primers	VHPS-110	
Sequence-based reagent	GAPDH (Primer)	Real-time primers	VHPS-3541	
Sequence-based reagent	HPRT1 (Primer)	Real-time primers	VHPS-4263	
Commercial assay or kit	Pierce ECL western blotting substrate	Thermo Fisher Scientific	Cat #32106	
Commercial assay or kit	Pierce BCA protein quantification assay	Thermo Fisher Scientific	Cat #23225	
Commercial assay or kit	RNeasy Plus Mini Kit	QIAGEN	Ref 74136	
Commercial assay or kit	Superscript III First-Strand Synthesis	Thermo Fisher Scientific	Ref 18080051	
Commercial assay or kit	SYBR Green PCR Master Mix	Applied Biosystems	Ref 4309155	
Commercial assay or kit	Lipofectamine LTX with PLUS reagent	Invitrogen	Ref 15338100	
Commercial assay or kit	QuickChange II XL Site-Directed Mutagenesis	Agilent Technologies	Cat #200522	
Chemical compound, drug	Fura-2 LR AM	ION Biosciences	1061E	
Chemical compound, drug	Thapsigargin	Enzo Life Sciences	BML-PE180-0001	
Chemical compound, drug	Cyclopiazonic acid	Cayman Chemical	11326	
Chemical compound, drug	Pluronic F-127	Sigma-Aldrich	P2443	
Chemical compound, drug	Imatinib	Sigma-Aldrich	CDS022173	
Software, algorithm	GraphPad Prism	Dotmatics	RRID:SCR_002798	
Software, algorithm	Microsoft Excel	Microsoft	RRID:SCR_016137	

DNA constructs

Bacterial expression vectors

Wild-type human CRT (accession number P27797) and CRT$_{Del52}$ described earlier (***Venkatesan et al., 2021a***) was expressed as a fusion protein with the B1 domain of streptococcal protein G (GB1) (***Huth et al., 1997***) and hexa-histidine tag using the pGB1 vector via ligation-independent cloning, as described earlier (***Del Cid et al., 2010***; ***DelProposto et al., 2009***). Using the pGB1-h*CALR* plasmid as a template, constructs for expressing his-tagged CRT$_{(1–351)}$ and CRT$_{(1–339)}$ truncation mutants were generated using QuikChange Site-Directed Mutagenesis Kit (Agilent Technologies) following the manufacturer's protocol and using primers indicated in the ***Supplementary file 1A***.

CRT knockdown

The single-guide RNA (sgRNA) for CRT knockdown was designed to target the GGCCACAGATGT CGGGACCT sequence found at the boundary of intron 3 and exon 4 of the *CALR* gene (***Mohan et al., 2020***). The primers for cloning of sgRNA into pLentiCRISPRv2-BLAST (pLB) vector (RRID:Addgene_98293) are given in the ***Supplementary file 1A***.

pSIP vectors for CRT expression in human cells

The pMSCV constructs (RRID:Addgene 75085) used for expression of wild-type CRT and the CRT_{Del52} described earlier (***Venkatesan et al., 2021a***) were used as templates to subclone wild-type *CALR* and $CALR_{Del52}$ cDNA sequences into the pSIP-*ZsGreen* (pLVX-SFFV-IRES-Puro) vector (RRID:Addgene_180278; ***Bashirova et al., 2020***) at the EcoRI and NotI sites using primers given in the ***Supplementary file 1A***. The cloning of *CALR* genes at the EcoRI and NotI sites within the pSIP-*ZsGreen* vector resulted in the removal of a fragment carrying *ZsGreen* so that the transduced cells did not express ZsGreen.

gRNA-resistant versions for reconstitution of CALR expression in KO cells

Silent mutations were introduced into the target sequence for sgRNA in the pSIP-$CALR_{WT}$ and pSIP-$CALR_{Del52}$ constructs by site-directed mutagenesis to make them resistant to Cas9-mediated editing. The QuikChange II XL Site-Directed Mutagenesis Kit (Agilent) was used along with primers listed in the ***Supplementary file 1A***. The PCR reaction was set up according to the manufacturer's protocol, followed by DpnI treatment for 1 hr at 37°C to digest the parental DNA strand. The DpnI-treated product was used to transform XL10-Gold ultracompetent cells. Two sets of primers were used to introduce a total of six silent mutations: C1QF and C1QR primers were used in the first round, and C2QF and C2QR primers were used to introduce further mutations into the DNA templates generated from the first round of mutagenesis.

Addition of a KDEL sequence into CRT_{Del52}

The pSIP-$CALR_{Del52\text{-}KDEL}$ construct containing a C-terminal KDEL motif was generated using sgRNA-resistant pSIP-$CALR_{Del52}$ construct as a template and primers given in ***Supplementary file 1A***. The amplicons were cloned at the EcoRI and NotI sites in the pSIP vector. The cloning of *CALR* genes at the EcoRI and NotI sites within the pSIP-*ZsGreen* vector resulted in the removal of a fragment carrying *ZsGreen* so that the transduced cells did not express ZsGreen.

Cell culture, viral transduction, and reconstitution of the expression of CRT mutants

Megakaryoblastic leukemia cell line (MEG-01) (RRID:CVCL_0425) from ATCC and HEK 293T cell lines (RRID:CVCL_0063) were cultured and maintained in RPMI 1640 and DMEM media, respectively, supplemented with 10% heat-inactivated fetal bovine serum (FBS, Gibco), antibiotic/antimycotic solution containing penicillin, streptomycin, and amphotericin (15240062), respectively, at 37°C, 5% CO_2, and 95% humidity. Wild-type CRT was knocked out in MEG-01 cells and HEK293T cells (CRT-KO) using Cas9 and sgRNA targeting GGCCACAGATGTCGGGACCT sequence within the *CALR* gene. For CRISPR/Cas9-mediated CRT knockdown, the HEK293T cells were first transfected with the lentiviral construct containing CRT-targeting sgRNA (pLB-CALR sgRNA) or the empty pLB vector along with the psPAX2 (RRID:Addgene_12260) and MD2.G (RRID:Addgene_12259) vectors using Lipofectamine LTX with PLUS reagent (Invitrogen) to make lentivirus. The lentivirus-containing media were harvested, filtered with 0.45 µm syringe filters, and added onto the target cells (MEG-01 or HEK293T cells) for infection. The MEG-01 cells were infected by spinoculation at 2500 rpm for 2 hr at room temperature in the presence of polybrene (8 µg/mL), followed by the replacement of 80% of virus-containing media with fresh complete media.

For HEK293T cells, the harvested viral supernatant was added to HEK 293T cells and incubated for 2 hr at 37°C, after which 80% of the viral suspension was replaced with complete growth media. Virus-containing media was completely replaced with fresh growth media 24 hr after infection, and the drug selection started with 2.5 µg/mL blasticidin 48 hr post-infection. Following drug selection, the CRT-KO cells were plated at a dilution of one cell per well in a 96-well plate to isolate single-cell clones.

The selected single-cell clones of CRT-KO MEG-01 and HEK293T cells were subsequently reconstituted with wild-type human CRT, CRT_{Del52}, or CRT_{Del52} with a C-terminal KDEL sequence using the respective sgRNA-resistant pSIP constructs and the same method of transduction explained above. The cells transduced with the empty pSIP vector without *ZsGreen* (***Supplementary file 1A***) were also generated to serve as control cells. Cells expressing CRT proteins or those containing empty pSIP vector were selected with 2 µg/mL puromycin. Selected cells were expanded and used for ER calcium

measurements. Both MEG-01 and HEK293T cells were authenticated by Labcorp using STR genotyping and routinely screened for mycoplasma contamination before use.

Protein expression and purification

The B1 domain of streptococcal protein G (GB1) and his-tagged versions of wild-type CRT, $CRT_{(1–351)}$, $CRT_{(1–339)}$, and CRT_{Del52} were cloned into the pGB1 vector (***DelProposto et al., 2009***). Chemically competent Origami B(DE3) *E. coli* cells were transformed with the pGB1 constructs of wild-type CRT, $CRT_{(1–351)}$, $CRT_{(1–339)}$, and CRT_{Del52}. Single colonies were grown overnight at 37°C. The overnight cultures were inoculated into larger (1–2 L) volumes of LB media and grown in a shaking incubator at 220 rpm and 37°C until the OD_{600} reached 0.8. Protein expression was then induced with 200 µM IPTG, and the cultures were further incubated at 16°C overnight on shaking. The bacterial cells were harvested, pelleted, and lysed in 50 mL of HEPES buffer containing (20 mM HEPES pH 7.5, 140 mM NaCl, 1 mM $CaCl_2$) by sonication. The lysates were clarified by centrifugation at 10,000 rpm, 4°C for 30 min. The supernatant was incubated with nickel-NTA resin (QIAGEN, 1018244) for 3 hr at 4°C and purified through a gravity-flow column. The unbound proteins and contaminants were removed by washing with a wash buffer containing 20 mM HEPES pH 7.5, 140 mM NaCl, 1 mM $CaCl_2$, and 10 mM imidazole. The his-tagged GB1-CRT proteins were eluted with buffer containing 20 mM HEPES pH 7.5, 140 mM NaCl, 1 mM $CaCl_2$, and 350 mM imidazole. The eluted proteins were concentrated and subjected to fast protein liquid chromatography over a Superdex 200 Increase 10/300 GL column at 4°C in 20 mM HEPES pH 7.5, 140 mM NaCl, 1 mM $CaCl_2$ as described previously (***Del Cid et al., 2010***; ***Wijeyesakere et al., 2011***). Monomer fractions, collected between 14 and 20 mL as shown in ***Figure 2***, were pooled, dialyzed, and concentrated to 4 mg/mL in 20 mM HEPES, 10 mM NaCl, 1 mM $CaCl_2$ pH 7.5 using Amicon Ultra concentrators with a molecular weight cutoff of 30,000 Da (Millipore) and frozen in 10% glycerol for further use.

Isothermal titration calorimetry

ITC measurements were done using the Nano-ITC SV (TA Instruments). Purified GB1-CRT monomers were dialyzed into 20 mM HEPES, 10 mM NaCl pH 7.5, brought to a concentration of 100 µM, and then pre-incubated with 50–100 µM $CaCl_2$ in 20 mM HEPES, 10 mM NaCl pH 7.5 for 30 min to block the high-affinity calcium-binding sites. This was followed by 25 sequential 10 µL injections of 20 mM HEPES, 10 mM NaCl, 10 mM $CaCl_2$ pH 7.5 into the protein solution maintained at 37°C in a total volume of 1.3 mL to final $CaCl_2$ concentrations of 1.6–1.7 mM. The heat changes measured for the sequential injections were curve-fitted to calculate the enthalpies, stoichiometries, and the dissociation constants using NanoAnalyze software.

Cytosolic calcium measurement and SOCE induction

MEG-01 cells and their *CALR*-modified versions were plated on glass coverslips pretreated with 0.01% poly-L-lysine to facilitate cell attachment. In separate experiments, cells were treated with 10 µM Imatinib (Sigma), a tyrosine kinase inhibitor, for 2 hr prior to cytosolic calcium measurements. Cells were loaded with 2.5 µM Fura-2/AM dye (Ion Biosciences) supplemented with 0.1% pluronic acid in a physiological salt solution (PSS) containing 140 mM NaCl, 2 mM $CaCl_2$, 5 mM KCl, 2 mM $MgCl_2$, 10 mM HEPES, and 11 mM glucose, and incubated for 60 min at 37°C. Live single-cell imaging was done at ×20 magnification using an Olympus IX71 inverted microscope equipped with a TILL Polychrome V monochromator light source, a Dual-View emission beam splitter, and a cooled Photometrics Quant-EM camera. Cells were transferred to a perfusion chamber that was mounted on the microscope stage, and PSS with or without 2 mM $CaCl_2$ was flowed over cells using a gravity-fed perfusion system. Cytosolic calcium measurements were performed by perfusing Fura-2-loaded cells in the chamber with 2 mM Ca^{2+}, followed by the addition of 25 µM CPA (Cayman) into the imaging buffer. To determine cytosolic calcium levels after activating SOCE, cells were initially perfused with Ca^{2+}-free PSS containing 0.1 mM EGTA, followed by the addition of 25 µM CPA in Ca^{2+}-free PSS and subsequent addition of 2 mM Ca^{2+} and 25 µM CPA in PSS (without EGTA) to reestablish calcium influx. The emission signals corresponding to the 340 and 380 nm excitation were recorded, and the signals resulting from 340/380 nm excitation were calculated using the Meta Fluor software. The basal cytosolic calcium was defined as the 340/380 nm signal ratio before CPA treatment (measured over a 4 or 5 min interval immediately before CPA addition). The fractional increase in cytosolic calcium

levels after ER Ca^{2+} depletion with CPA was calculated as the difference between peak signal (single time point) and baseline (averaged over a 4 or 5 min interval before CPA addition), as a ratio relative to the baseline. The fractional increase in cytosolic calcium after addition of 2 mM extracellular Ca^{2+} and CPA was calculated as the difference between the peak signal following Ca^{2+} and CPA addition (averaged over a 1 min time interval following the peak signal) and the baseline (the signal averaged over a 0.8–1 min interval immediately before the Ca^{2+} and CPA addition) relative to the baseline. Total calcium release after ER Ca^{2+} depletion was reported as the total area under the curve (AUC). Fractional increases were calculated as (Peak–Baseline)/Baseline × 100. This was calculated as peak signals after CPA addition relative to the baseline before CPA (measured over a 4 or 5 min interval immediately before CPA addition).

ER calcium measurements in HEK293T cells

CALR-modified HEK cells as described in Materials and methods were transiently transfected with pCIS-GEM-CEPIA1er (RRID:Addgene_58217; ***Suzuki et al., 2014***) using Fugene HD reagent (Promega). The transfected cells were harvested after 72 hr. Cells were washed twice with FACS buffer (phosphate-buffered saline [PBS]+2% FBS) supplemented with 2 mM Ca^{2+} and resuspended in the same FACS buffer. The live-dead stain 7-AAD (BD, 559925; RRID:AB_286926) was added at 1:200 dilution and the cells were analyzed by flow cytometry using the BD LSRFortessa cell analyzer. The signal for the Ca^{2+}-bound GEM-CEPIA1er probe was recorded in the Pacific Blue channel (excitation at 405 nm and emission at 452–455 nm) and the signal for the unbound GEM-CEPIA1er probe was recorded in the AmCyan channel (excitation at 405 and emission at 498 nm). The analysis of flow cytometry data was done using the FlowJo software (v10.10.00;RRID:SCR_008520). The cells were gated based on the forward (FSC-A) and side scatter (SSC-A), followed by gating on the 7AAD-negative (live) cells, and subsequent gating on the cells positive for the expression of GEM-CEPIA1er probe measured in the Pacific Blue and AmCyan channels. Basal signals were initially recorded, followed by the addition of 5 µM thapsigargin (Tg) and subsequent recording of signals for the treated and untreated cells at four different time points between 2 and 10 min. The ratio of mean fluorescence intensity of the bound to the unbound signal was used for calculations. In additional experiments, ER calcium levels were measured by spectrofluorimetry in HEK cells transfected with pCIS-GEM-CEPIA1er. Fluorescence emission spectra were recorded between 420 and 600 nm, following excitation at 390 nm. Basal spectra were initially recorded using 3 million cells suspended in PBS containing 2 mM Ca^{2+}, followed by treatment with 5 µM Tg, and additional spectra were recorded at 3 min intervals (3–15) min. The ratios of mean fluorescence intensities of the bound (~460 nm) to unbound (~510 nm) peak signals were calculated in the absence of Tg or at 15 min following Tg addition to compare the basal signals and the changes following Tg addition.

Immunoblotting

The HEK293T and MEG-01 cells were harvested and lysed in lysis buffer (50 mM Tris pH 7.5, 150 mM NaCl, 1% Triton X-100, 5 mM $CaCl_2$) for 30 min at 4°C. The lysates were clarified by centrifugation, and the total amount of protein in the lysates was determined using the BCA reagent kit (Thermo Scientific). The volume of lysate containing 20–40 µg of protein was denatured by boiling in 1× SDS loading dye for 5 min and subjected to SDS-PAGE. Following electrophoresis, the proteins were transferred onto a PVDF membrane. The membranes were blocked in 5% non-fat dry milk solution in TBST (Tris-buffered saline with Tween-20), followed by immunoblotting and detection for protein expression using primary anti-CRT(N) antibody (Cell Signaling Technology [CST] 12238; RRID:AB_2688013; 1:10,000 dilution) for detection of CRT_{WT} and anti-CRT(C-mut) antibody for detection of CRT mutants (***Venkatesan et al., 2021a***). Primary anti-STAT5 (94205S, RRID:AB_2737403; 1:1000), anti-phospho-STAT5 (93559S, RRID:AB_823649; 1:1000), anti-GRP78/BiP (11587-1-AP, RRID:AB_2119855; 1:10,000), anti-GRP94 (14700-1-AP, RRID:AB_2233347; 1:10,000), anti-ERp57 (15967-1-AP, RRID:AB_2236784; 1:10,000), and anti-PDIA6 (18233-1-AP, RRID:AB_10805765; 1:20,000) were used to probe for the expression of BiP, GRP94, PDIA3, and PDIA6, respectively. Anti-GAPDH (CST 2118, RRID:AB_561053; 1:20,000) and anti-vinculin (CST 13901, RRID:AB_2728768; 1:20,000) were used to probe for GAPDH and vinculin as loading controls. Blots were incubated with horseradish peroxidase-conjugated secondary antibodies (Jackson ImmunoResearch) and developed by chemiluminescence (Pierce ECL

western blotting substrate, 32106). Immunoblot images were captured using the Azure 300 Chemi Imager (Azure Biosystems).

RNA sequencing

The parental and CRT-KO MEG-01 cells were grown in complete media for 12–18 hr before harvesting. Total RNA was isolated using the RNeasy Plus Mini Kit (QIAGEN). This was followed by poly-A selection and enrichment of mRNA using NEB Next Ultra Express RNA kit and a NEB Poly A kit (New England Biolabs). Sequencing was done on the NovaSeq at PE150, targeting 30–40 million reads/sample after cDNA library preparation. Data were pre-filtered to remove genes with zero counts in all samples. Differential gene expression analysis was performed using DESeq2 (RRID:SCR_015687). The differentially expressed genes were selected as those with a $\log_2$ fold-change of <-0.49 or >0.49 and p-values<0.05. The results from RNA sequencing were further analyzed in the iPathwayGuide to identify significantly altered proteins related to calcium signaling. The volcano plot was plotted in GraphPad Prism as $\log_2$ fold-change (x-axis) vs. $-\log_{10}$ adjusted p-value.

Real-time PCR

Total RNA was isolated using the RNeasy Plus Mini Kit (QIAGEN) followed by synthesis of complementary DNA using the Superscript III First-Strand Synthesis Kit (Thermo Fisher Scientific) following the manufacturer's protocol. Quantitative RT-PCR was performed on the ABI 7500 FAST Real-Time PCR machine (Thermo Fisher Scientific, USA) using the SYBR Green PCR Master mix (Applied Biosystems, UK) and gene-specific primers (***Supplementary file 1B***). Measurement was done in technical duplicates. The expression of target genes was quantified using the $2^{-\Delta\Delta Ct}$ method and normalized to the expression of either one or multiple endogenous control genes, including beta-actin (ACTB), glyceraldehyde 3-phosphate dehydrogenase (GAPDH), and hypoxanthine phosphoribosyltransferase 1 (HPRT1). The expression of the target gene in MEG-01 CRT-KO and wild-type and CRT_{Del52} reconstitution cells was further normalized to the mean expression of parental MEG-01 or CRT-KO-Vec. The calculated relative mRNA transcript expression values (RQ) were plotted using GraphPad Prism.

Statistical analysis

All data were compiled using Microsoft Excel (RRID:SCR_016137). A paired, two-tailed Student's t-test analysis was done to compare mean differences between two groups, while a one-way ANOVA was done to compare mean differences among more than two groups. These analyses were done using GraphPad Prism 10.4 (RRID:SCR_002798) statistical package. The threshold for statistical significance was observed at a p-value$\leq$0.05.

Acknowledgements

We thank Grace Pagnucco for generating the CRISPR/Cas9-engineered HEK293T CRT-KO cells and Arunkumar Venkatesan for generating the MEG-01 CRT-KO cells. We would like to extend special thanks and appreciation to Chante Liu and Mathewos Biniam Tebeje from the Satin lab for their support with microscopic calcium measurements. We thank Luis Teran-Rodriguez for assistance with data analysis and Dr. Sivaraj Sivaramakrishnan for many helpful suggestions. We thank the Advanced Genomic Core (ACG) at the University of Michigan for conducting the library preparation and next-generation sequencing, as well as Rebecca Tagett and the Bioinformatics Core of the University of Michigan Medical School for conducting the RNA sequencing data analysis. We thank Dr. Arthur Sherman for many insightful comments. This work was funded by the National Institutes of Health grants (R01 AI123957 to MR and R01 DK46409 to LSS) and by the University of Michigan Fast Forward Protein Folding Diseases Initiative.

Additional information

Funding

Funder	Grant reference number	Author
National Institute of Allergy and Infectious Diseases	AI123957	Malini Raghavan
National Institute of Diabetes and Digestive and Kidney Diseases	DK46409	Leslie S Satin

The funders had no role in study design, data collection and interpretation, or the decision to submit the work for publication.

Author contributions

Ishmael Nii Ayibontey Tagoe, Investigation, Visualization, Methodology, Writing – original draft, Writing – review and editing; Amanpreet Kaur, Investigation, Visualization, Writing – review and editing; Osbourne Quaye, Emmanuel Ayitey Tagoe, Supervision, Writing – review and editing; Nicole M Koropatkin, Resources, Formal analysis, Supervision, Methodology, Writing – review and editing; Leslie S Satin, Resources, Formal analysis, Supervision, Funding acquisition, Methodology, Writing – review and editing; Malini Raghavan, Conceptualization, Resources, Formal analysis, Supervision, Funding acquisition, Visualization, Methodology, Writing – original draft, Project administration, Writing – review and editing

Author ORCIDs

Ishmael Nii Ayibontey Tagoe https://orcid.org/0009-0003-4511-6410
Amanpreet Kaur https://orcid.org/0000-0001-6806-8448
Osbourne Quaye https://orcid.org/0000-0002-0621-876X
Emmanuel Ayitey Tagoe https://orcid.org/0000-0001-7179-1872
Nicole M Koropatkin https://orcid.org/0000-0002-2459-3336
Leslie S Satin https://orcid.org/0000-0003-1355-8647
Malini Raghavan https://orcid.org/0000-0002-1345-9318

Peer review material

Version of Record:
Reviewer #1 (Public review): https://doi.org/10.7554/eLife.109647.3.sa1
Reviewer #2 (Public review): https://doi.org/10.7554/eLife.109647.3.sa2
Author response https://doi.org/10.7554/eLife.109647.3.sa3

Reviewed preprint v2
Reviewer #1 (Public review): https://doi.org/10.7554/eLife.109647.2.sa2
Reviewer #2 (Public review): https://doi.org/10.7554/eLife.109647.2.sa1
Author response: https://doi.org/10.7554/eLife.109647.2.sa0
eLife Assessment https://doi.org/10.7554/eLife.109647.2.sa3

Reviewed preprint v1
Reviewer #1 (Public review): https://doi.org/10.7554/eLife.109647.1.sa2
Reviewer #2 (Public review): https://doi.org/10.7554/eLife.109647.1.sa1
Author response: https://doi.org/10.7554/eLife.109647.1.sa0
eLife Assessment https://doi.org/10.7554/eLife.109647.1.sa3

Additional files

Supplementary files

MDAR checklist

Supplementary file 1. List of primers used in this study for cloning, site-directed mutagenesis, and qPCR.

Data availability

RNA sequencing gene expression data is available in the GEO database with accession number GSE296671.All source data for all Figures can be accessed at https://www.immport.org/ under study accession ID SDY3677.

The following datasets were generated:

Author(s)	Year	Dataset title	Dataset URL	Database and Identifier
Tagoe INA, Kaur A, Raghavan M	2026	Differential gene expression in the MEG-01 Megakaryoblast Cell Line (ATCC CRL-2021) with and without calreticulin knockout	https://www.ncbi.nlm.nih.gov/geo/query/acc.cgi?acc=GSE296671	NCBI Gene Expression Omnibus, GSE296671
Tagoe I, Raghavan M	2026	SDY3677: Molecular and Functional Analysis of Calcium Binding by a Cancer-linked Calreticulin Mutant	https://doi.org/10.21430/M3IQGOHZUZ	ImmPort, 10.21430/M3IQGOHZUZ

The following previously published datasets were used:

Author(s)	Year	Dataset title	Dataset URL	Database and Identifier
Tank K, Wu L, Hu L, Xue T, Jin Y, Zhou X, Luo C, Zhao Y, Tong L, Dai J, Feng D, Zeng Z, Pan D	2025	Perturbation of calreticulin potentiates CD8+ T cell-mediated antitumor immunity	https://www.ncbi.nlm.nih.gov/geo/query/acc.cgi?acc=GSE285113	NCBI Gene Expression Omnibus, GSE285113
Fosselteder J, Pabst G, Sconocchia T, Schlacher A, Auinger L, Kashofer K, Kashofer K, Beham-Schmid C, Trajanoski S, Waskow C, Scholl W, Sill H, Zebisch A, Wolfler A, Thomas D, Reinisch A	2023	Human gene-engineered calreticulin mutant stem cells recapitulate MPN hallmarks and identify targetable vulnerabilities	https://www.ncbi.nlm.nih.gov/geo/query/acc.cgi?acc=GSE195705NCBI	NCBI Gene Expression Omnibus, GSE195705

References

Araki M, Yang Y, Masubuchi N, Hironaka Y, Takei H, Morishita S, Mizukami Y, Kan S, Shirane S, Edahiro Y, Sunami Y, Ohsaka A, Komatsu N. 2016. Activation of the thrombopoietin receptor by mutant calreticulin in CALR-mutant myeloproliferative neoplasms. *Blood* **127**:1307–1316. DOI: https://doi.org/10.1182/blood-2015-09-671172, PMID: 26817954

Arnaudeau S, Frieden M, Nakamura K, Castelbou C, Michalak M, Demaurex N. 2002. Calreticulin differentially modulates calcium uptake and release in the endoplasmic reticulum and mitochondria. *The Journal of Biological Chemistry* **277**:46696–46705. DOI: https://doi.org/10.1074/jbc.M202395200, PMID: 12324449

Arshad N, Cresswell P. 2018. Tumor-associated calreticulin variants functionally compromise the peptide loading complex and impair its recruitment of MHC-I. *The Journal of Biological Chemistry* **293**:9555–9569. DOI: https://doi.org/10.1074/jbc.RA118.002836, PMID: 29769311

Bagur R, Hajnóczky G. 2017. Intracellular Ca^{2+} sensing: its role in calcium homeostasis and signaling. *Molecular Cell* **66**:780–788. DOI: https://doi.org/10.1016/j.molcel.2017.05.028, PMID: 28622523

Baksh S, Michalak M. 1991. Expression of calreticulin in *Escherichia coli* and identification of its Ca2+ binding domains. *The Journal of Biological Chemistry* **266**:21458–21465. DOI: https://doi.org/10.1016/S0021-9258(18)54661-5, PMID: 1939178

Bashirova AA, Viard M, Naranbhai V, Grifoni A, Garcia-Beltran W, Akdag M, Yuki Y, Gao X, O'hUigin C, Raghavan M, Wolinsky S, Bream JH, Duggal P, Martinson J, Michael NL, Kirk GD, Buchbinder SP, Haas D, Goedert JJ, Deeks SG, et al. 2020. HLA tapasin independence: broader peptide repertoire and HIV control. *PNAS* **117**:28232–28238. DOI: https://doi.org/10.1073/pnas.2013554117

Bastianutto C, Clementi E, Codazzi F, Podini P, De Giorgi F, Rizzuto R, Meldolesi J, Pozzan T. 1995. Overexpression of calreticulin increases the Ca2+ capacity of rapidly exchanging Ca2+ stores and reveals aspects of their lumenal microenvironment and function. *The Journal of Cell Biology* **130**:847–855. DOI: https://doi.org/10.1083/jcb.130.4.847, PMID: 7642702

Bhuria V, Franz T, Baldauf C, Böttcher M, Chatain N, Koschmieder S, Brümmendorf TH, Mougiakakos D, Schraven B, Kahlfuß S, Fischer T. 2024. Activating mutations in JAK2 and CALR differentially affect intracellular calcium flux in store operated calcium entry. *Cell Communication and Signaling* **22**:186. DOI: https://doi.org/10.1186/s12964-024-01530-z, PMID: 38509561

Biswas C, Ostrovsky O, Makarewich CA, Wanderling S, Gidalevitz T, Argon Y. 2007. The peptide-binding activity of GRP94 is regulated by calcium. *The Biochemical Journal* **405**:233–241. DOI: https://doi.org/10.1042/BJ20061867, PMID: 17411420

Cabanas H, Harnois T, Magaud C, Cousin L, Constantin B, Bourmeyster N, Déliot N. 2018. Deregulation of calcium homeostasis in Bcr-Abl-dependent chronic myeloid leukemia. *Oncotarget* **9**:26309–26327. DOI: https://doi.org/10.18632/oncotarget.25241, PMID: 29899861

Chachoua I, Pecquet C, El-Khoury M, Nivarthi H, Albu RI, Marty C, Gryshkova V, Defour JP, Vertenoeil G, Ngo A, Koay A, Raslova H, Courtoy PJ, Choong ML, Plo I, Vainchenker W, Kralovics R, Constantinescu SN. 2016. Thrombopoietin receptor activation by myeloproliferative neoplasm associated calreticulin mutants. *Blood* **127**:1325–1335. DOI: https://doi.org/10.1182/blood-2015-11-681932, PMID: 26668133

Del Cid N, Jeffery E, Rizvi SM, Stamper E, Peters LR, Brown WC, Provoda C, Raghavan M. 2010. Modes of calreticulin recruitment to the major histocompatibility complex class I assembly pathway. *The Journal of Biological Chemistry* **285**:4520–4535. DOI: https://doi.org/10.1074/jbc.M109.085407, PMID: 19959473

DelProposto J, Majmudar CY, Smith JL, Brown WC. 2009. Mocr: a novel fusion tag for enhancing solubility that is compatible with structural biology applications. *Protein Expression and Purification* **63**:40–49. DOI: https://doi.org/10.1016/j.pep.2008.08.011, PMID: 18824232

Di Buduo CA, Abbonante V, Marty C, Moccia F, Rumi E, Pietra D, Soprano PM, Lim D, Cattaneo D, Iurlo A, Gianelli U, Barosi G, Rosti V, Plo I, Cazzola M, Balduini A. 2020. Defective interaction of mutant calreticulin and SOCE in megakaryocytes from patients with myeloproliferative neoplasms. *Blood* **135**:133–144. DOI: https://doi.org/10.1182/blood.2019001103, PMID: 31697806

Foßelteder J, Pabst G, Sconocchia T, Schlacher A, Auinger L, Kashofer K, Beham-Schmid C, Trajanoski S, Waskow C, Schöll W, Sill H, Zebisch A, Wölfler A, Thomas D, Reinisch A. 2023. Human gene-engineered calreticulin mutant stem cells recapitulate MPN hallmarks and identify targetable vulnerabilities. *Leukemia* **37**:843–853. DOI: https://doi.org/10.1038/s41375-023-01848-6, PMID: 36813992

Han L, Schubert C, Köhler J, Schemionek M, Isfort S, Brümmendorf TH, Koschmieder S, Chatain N. 2016. Calreticulin-mutant proteins induce megakaryocytic signaling to transform hematopoietic cells and undergo accelerated degradation and Golgi-mediated secretion. *Journal of Hematology & Oncology* **9**:45. DOI: https://doi.org/10.1186/s13045-016-0275-0

Hendershot LM, Buck TM, Brodsky JL. 2024. The essential functions of molecular chaperones and folding enzymes in maintaining endoplasmic reticulum homeostasis. *Journal of Molecular Biology* **436**:168418. DOI: https://doi.org/10.1016/j.jmb.2023.168418, PMID: 38143019

Huth JR, Bewley CA, Jackson BM, Hinnebusch AG, Clore GM, Gronenborn AM. 1997. Design of an expression system for detecting folded protein domains and mapping macromolecular interactions by NMR. *Protein Science* **6**:2359–2364. DOI: https://doi.org/10.1002/pro.5560061109, PMID: 9385638

Ibarra J, Elbanna YA, Kurylowicz K, Ciboddo M, Greenbaum HS, Arellano NS, Rodriguez D, Evers M, Bock-Hughes A, Liu C, Smith Q, Lutze J, Baumeister J, Kalmer M, Olschok K, Nicholson B, Silva D, Maxwell L, Dowgielewicz J, Rumi E, et al. 2022. Type I but Not Type II calreticulin mutations activate the IRE1α/XBP1 pathway of the unfolded protein response to drive myeloproliferative neoplasms. *Blood Cancer Discovery* **3**:298–315. DOI: https://doi.org/10.1158/2643-3230.BCD-21-0144, PMID: 35405004

Kaur A, Desikan H, Pagnucco G, Kandarpa M, Talpaz M, Raghavan M. 2025. Effects of calreticulin mutations on HLA Class I expression in myeloproliferative neoplasms. [*bioRxiv*]. DOI: https://doi.org/10.1101/2025.06.24.661416, PMID: 40667261

Klampfl T, Gisslinger H, Harutyunyan AS, Nivarthi H, Rumi E, Milosevic JD, Them NCC, Berg T, Gisslinger B, Pietra D, Chen D, Vladimer GI, Bagienski K, Milanesi C, Casetti IC, Sant'Antonio E, Ferretti V, Elena C, Schischlik F, Cleary C, et al. 2013. Somatic mutations of calreticulin in myeloproliferative neoplasms. *The New England Journal of Medicine* **369**:2379–2390. DOI: https://doi.org/10.1056/NEJMoa1311347, PMID: 24325356

Li Y, Camacho P. 2004. Ca2+-dependent redox modulation of SERCA 2b by ERp57. *The Journal of Cell Biology* **164**:35–46. DOI: https://doi.org/10.1083/jcb.200307010, PMID: 14699087

Li J, Prins D, Park HJ, Grinfeld J, Gonzalez-Arias C, Loughran S, Dovey OM, Klampfl T, Bennett C, Hamilton TL, Pask DC, Sneade R, Williams M, Aungier J, Ghevaert C, Vassiliou GS, Kent DG, Green AR. 2018. Mutant calreticulin knockin mice develop thrombocytosis and myelofibrosis without a stem cell self-renewal advantage. *Blood* **131**:649–661. DOI: https://doi.org/10.1182/blood-2017-09-806356, PMID: 29282219

Lièvremont JP, Rizzuto R, Hendershot L, Meldolesi J. 1997. BiP, a major chaperone protein of the endoplasmic reticulum lumen, plays a direct and important role in the storage of the rapidly exchanging pool of Ca2+. *The Journal of Biological Chemistry* **272**:30873–30879. DOI: https://doi.org/10.1074/jbc.272.49.30873, PMID: 9388233

Liu P, Zhao L, Loos F, Marty C, Xie W, Martins I, Lachkar S, Qu B, Waeckel-Énée E, Plo I, Vainchenker W, Perez F, Rodriguez D, López-Otin C, van Endert P, Zitvogel L, Kepp O, Kroemer G. 2020. Immunosuppression by mutated calreticulin released from malignant cells. *Molecular Cell* **77**:748–760. DOI: https://doi.org/10.1016/j.molcel.2019.11.004

Macer DRJ, Koch GLE. 1988. Identification of a set of calcium-binding proteins in reticuloplasm, the luminal content of the endoplasmic reticulum. *Journal of Cell Science* **91**:61–70. DOI: https://doi.org/10.1242/jcs.91.1.61

Marty C, Pecquet C, Nivarthi H, El-Khoury M, Chachoua I, Tulliez M, Villeval JL, Raslova H, Kralovics R, Constantinescu SN, Plo I, Vainchenker W. 2016. Calreticulin mutants in mice induce an MPL-dependent thrombocytosis with frequent progression to myelofibrosis. *Blood* **127**:1317–1324. DOI: https://doi.org/10.1182/blood-2015-11-679571, PMID: 26608331

Marzec M, Eletto D, Argon Y. 2012. GRP94: An HSP90-like protein specialized for protein folding and quality control in the endoplasmic reticulum. *Biochimica et Biophysica Acta* **1823**:774–787. DOI: https://doi.org/10.1016/j.bbamcr.2011.10.013, PMID: 22079671

Masubuchi N, Araki M, Yang Y, Hayashi E, Imai M, Edahiro Y, Hironaka Y, Mizukami Y, Kihara Y, Takei H, Nudejima M, Koike M, Ohsaka A, Komatsu N. 2020. Mutant calreticulin interacts with MPL in the secretion pathway for activation on the cell surface. *Leukemia* **34**:499–509. DOI: https://doi.org/10.1038/s41375-019-0564-z, PMID: 31462733

Mery L, Mesaeli N, Michalak M, Opas M, Lew DP, Krause KH. 1996. Overexpression of calreticulin increases intracellular Ca2+ storage and decreases store-operated Ca2+ influx. *The Journal of Biological Chemistry* **271**:9332–9339. DOI: https://doi.org/10.1074/jbc.271.16.9332, PMID: 8621597

Michalak M. 2024. Calreticulin: endoplasmic reticulum Ca^{2+} gatekeeper. *Journal of Cellular and Molecular Medicine* **28**:e17839. DOI: https://doi.org/10.1111/jcmm.17839

Mohan HM, Yang B, Dean NA, Raghavan M. 2020. Calreticulin enhances the secretory trafficking of a misfolded α-1-antitrypsin. *The Journal of Biological Chemistry* **295**:16754–16772. DOI: https://doi.org/10.1074/jbc.RA120.014372, PMID: 32978262

Nakamura K, Zuppini A, Arnaudeau S, Lynch J, Ahsan I, Krause R, Papp S, De Smedt H, Parys JB, Muller-Esterl W, Lew DP, Krause KH, Demaurex N, Opas M, Michalak M. 2001. Functional specialization of calreticulin domains. *The Journal of Cell Biology* **154**:961–972. DOI: https://doi.org/10.1083/jcb.200102073, PMID: 11524434

Nangalia J, Massie CE, Baxter EJ, Nice FL, Gundem G, Wedge DC, Avezov E, Li J, Kollmann K, Kent DG, Aziz A, Godfrey AL, Hinton J, Martincorena I, Van Loo P, Jones AV, Guglielmelli P, Tarpey P, Harding HP, Fitzpatrick JD, et al. 2013. Somatic CALR mutations in myeloproliferative neoplasms with nonmutated JAK2. *The New England Journal of Medicine* **369**:2391–2405. DOI: https://doi.org/10.1056/NEJMoa1312542, PMID: 24325359

Ogura M, Morishima Y, Ohno R, Kato Y, Hirabayashi N, Nagura H, Saito H. 1985. Establishment of a novel human megakaryoblastic leukemia cell line, MEG- 01, with positive Philadelphia chromosome. *Blood* **66**:1384–1392. DOI: https://doi.org/10.1182/blood.V66.6.1384.1384

Okumura M, Kanemura S, Matsusaki M, Kinoshita M, Saio T, Ito D, Hirayama C, Kumeta H, Watabe M, Amagai Y, Lee YH, Akiyama S, Inaba K. 2021. A unique leucine-valine adhesive motif supports structure and function of protein disulfide isomerase P5 via dimerization. *Structure* **29**:1357–1370. DOI: https://doi.org/10.1016/j.str.2021.03.016, PMID: 33857433

Pecquet C, Papadopoulos N, Balligand T, Chachoua I, Tisserand A, Vertenoeil G, Nédélec A, Vertommen D, Roy A, Marty C, Nivarthi H, Defour JP, El-Khoury M, Hug E, Majoros A, Xu E, Zagrijtschuk O, Fertig TE, Marta DS, Gisslinger H, et al. 2023. Secreted mutant calreticulins as rogue cytokines in myeloproliferative neoplasms. *Blood* **141**:917–929. DOI: https://doi.org/10.1182/blood.2022016846, PMID: 36356299

Pietra D, Rumi E, Ferretti VV, Di Buduo CA, Milanesi C, Cavalloni C, Sant'Antonio E, Abbonante V, Moccia F, Casetti IC, Bellini M, Renna MC, Roncoroni E, Fugazza E, Astori C, Boveri E, Rosti V, Barosi G, Balduini A, Cazzola M. 2016. Differential clinical effects of different mutation subtypes in CALR-mutant myeloproliferative neoplasms. *Leukemia* **30**:431–438. DOI: https://doi.org/10.1038/leu.2015.277, PMID: 26449662

Prins D, Groenendyk J, Touret N, Michalak M. 2011. Modulation of STIM1 and capacitative Ca2+ entry by the endoplasmic reticulum luminal oxidoreductase ERp57. *EMBO Reports* **12**:1182–1188. DOI: https://doi.org/10.1038/embor.2011.173, PMID: 21941299

Putney JW. 2011. Origins of the concept of store-operated calcium entry. *Frontiers in Bioscience* **3**:980–984. DOI: https://doi.org/10.2741/202, PMID: 21622247

Schürch PM, Malinovska L, Hleihil M, Losa M, Hofstetter MC, Wildschut MHE, Lysenko V, Lakkaraju AKK, Maat CA, Benke D, Aguzzi A, Wollscheid B, Picotti P, Theocharides APA. 2022. Calreticulin mutations affect its chaperone function and perturb the glycoproteome. *Cell Reports* **41**:111689. DOI: https://doi.org/10.1016/j.celrep.2022.111689

Shivarov V, Ivanova M, Tiu RV. 2014. Mutated calreticulin retains structurally disordered C terminus that cannot bind Ca(2+): some mechanistic and therapeutic implications. *Blood Cancer Journal* **4**:e185. DOI: https://doi.org/10.1038/bcj.2014.7, PMID: 24562385

Sönnichsen B, Füllekrug J, Nguyen Van P, Diekmann W, Robinson DG, Mieskes G. 1994. Retention and retrieval: both mechanisms cooperate to maintain calreticulin in the endoplasmic reticulum. *Journal of Cell Science* **107**:2705–2717. DOI: https://doi.org/10.1242/jcs.107.10.2705, PMID: 7876339

Suzuki J, Kanemaru K, Ishii K, Ohkura M, Okubo Y, Iino M. 2014. Imaging intraorganellar Ca2+ at subcellular resolution using CEPIA. *Nature Communications* **5**:4153. DOI: https://doi.org/10.1038/ncomms5153, PMID: 24923787

Tang K, Wu L, Hu Y, Xue T, Jin Y, Zhou X, Luo C, Zhao Y, Tong L, Dai J, Feng D, Zeng Z, Pan D. 2025. Perturbation of calreticulin potentiates CD8+ T cell-mediated antitumor immunity. *The Journal of Experimental Medicine* **222**:e20242360. DOI: https://doi.org/10.1084/jem.20242360, PMID: 40833532

Venkatesan A, Geng J, Kandarpa M, Wijeyesakere SJ, Bhide A, Talpaz M, Pogozheva ID, Raghavan M. 2021a. Mechanism of mutant calreticulin-mediated activation of the thrombopoietin receptor in cancers. *Journal of Cell Biology* **220**:9179. DOI: https://doi.org/10.1083/jcb.202009179

Venkatesan A, Satin LS, Raghavan M. 2021b. Roles of calreticulin in protein folding, immunity, calcium signaling and cell transformation. *Progress in Molecular and Subcellular Biology* **59**:145–162. DOI: https://doi.org/10.1007/978-3-030-67696-4_7, PMID: 34050865

Wijeyesakere SJ, Gafni AA, Raghavan M. 2011. Calreticulin is a thermostable protein with distinct structural responses to different divalent cation environments. *The Journal of Biological Chemistry* **286**:8771–8785. DOI: https://doi.org/10.1074/jbc.M110.169193, PMID: 21177861

Wijeyesakere SJ, Bedi SK, Huynh D, Raghavan M. 2016. The C-terminal acidic region of calreticulin mediates phosphatidylserine binding and apoptotic cell phagocytosis. *Journal of Immunology* **196**:3896–3909. DOI: https://doi.org/10.4049/jimmunol.1502122, PMID: 27036911

Zhang IX, Raghavan M, Satin LS. 2020. The endoplasmic reticulum and calcium homeostasis in pancreatic beta cells. *Endocrinology* **161**:bqz028. DOI: https://doi.org/10.1210/endocr/bqz028, PMID: 31796960